Active tectonics around Almaty and along the Zailisky Alatau rangefront

Grützner, C.[1, 2]*; Walker, R. T.[3]; Abdrakhmatov, K. E.[4]; Mukambaev, A.[5]; Elliott, A. J.[3]; Elliott, J. R.[6]

1 COMET, Bullard Laboratories, Cambridge University, Madingley Road, Madingley Rise, Cambridge, CB3 0EZ

2 Now at: Institute of Geological Sciences, Friedrich Schiller University Jena, Burgweg 11, 07749 Jena, Germany

3 COMET, Dept. of Earth Sciences, Oxford University, South Parks Road, Oxford, OX1 3AN

4 Institute of Seismology, National Academy of Sciences, Kyrgyz Republic

5 Data Center of the Institute of Geophysical Researches, L. Chaikinoy Street 4, Almaty 050020, Kazakhstan

6 COMET, School of Earth & Environment, University of Leeds, LS2 9JT, UK

*Corresponding author: Christoph Grützner (christoph.gruetzner@uni-jena.de)

Keywords

Tien Shan, Zailisky Alatau, active tectonics, tectonic geomorphology, earthquakes & faulting

Highlights

- Post-LGM tectonic activity along the Almaty rangefront is expressed in fault scarps in alluvial fans, folding, uplifted abandoned river terraces, and backthrusts

- Active deformation is laterally distributed, affecting the rangefront, the interior of the mountains, and the foreland

- The Holocene slip rate of the rangefront fault is ~1.2-2.2 mm/a in the eastern section

Abstract

The Zailisky Alatau is a >250-km-long mountain range in Southern Kazakhstan. Its northern rangefront around the major city of Almaty has more than 4 km topographic relief, yet in contrast to other large mountain fronts in the Tien Shan, little is known about its Late Quaternary tectonic activity despite several destructive earthquakes in the historical record. We analyse the tectonic geomorphology of the rangefront fault using field observations, differential GPS measurements of fault scarps, historical and recent satellite imagery, metre-scale topography derived from stereo satellite images, and decimetre-scale elevation models from UAV surveys. Fault scarps ranging in height from ~2 m to >20 m in alluvial fans indicate surface rupturing earthquakes occurred along the rangefront fault since the Last Glacial Maximum (LGM). Minimum estimated magnitudes for those earthquakes are M6.8-7. Radiocarbon dating results from charcoal layers in uplifted river terraces indicate a Holocene slip rate of ~1.2-2.2 mm/a. We find additional evidence for active tectonic deformation all along the Almaty rangefront, basinward in the Kazakh platform, and in the interior of the Zailisky mountain range. Our data indicate the seismic hazard faced by Almaty comes from a variety of sources, and we emphasize the problems related to urban growth into the loess-covered foothills and secondary earthquake effects. With our structural and geochronologic framework we present a schematic evolution of the Almaty rangefront that may be applicable to similar settings of tectonic shortening in the mountain ranges of Central Asia.

1. Introduction

Almaty, the former capital of Kazakhstan and today expanding as the home to more than 1.7 million people, lies at the foothills of the Zailisky Alatau (Alatau: “coloured mountains” in Kyrgyz). These mountains separate Lake Issyk-Kul in the south from the Kazakh platform to the north and form the northernmost range of the Tien Shan at this longitude (Fig. 1a). Although being rather young – modern Almaty was founded as Verny in the 19th Century as a Russian garrison--the city has suffered from several strong and destructive earthquakes (Fig. 1b). In 1887, the Verny Earthquake with a magnitude of about 7.3 had its epicentre a few kilometers west of the city. The precise location is unknown since the earthquake occurred in the pre-instrumental era and no surface ruptures were reported [*Tatevossian*, 2007]. The earthquake triggered numerous landslides [*Mushketov*, 1890] and led to several hundred fatalities [*Hay*, 1888]. Only two years later, in 1889, the Chilik Earthquake, with a magnitude of ~8, ruptured the surface 100 km to the southeast of Almaty and led to severe shaking in the city [*Krüger et al.*, 2015; *Abdrakhmatov et al.*, 2016]. This earthquake produced ~175 km of surface ruptures and up to 10 m of surface slip [*Abdrakhmatov et al.*, 2016] (Fig. 1b). Finally, Almaty was heavily damaged by the 1911 Chon Kemin Earthquake, with a magnitude of ~8, which occurred on the southern flank of the Zailisky Alatau [*Delvaux et al.*, 2001; *Kulikova et al.*, 2015; *Arrowsmith et al.*, 2017]. Up to ~200 km of surface ruptures and more than 10 m of slip resulted from this event [*Arrowsmith et al.*, 2017] (Fig. 1b). *Kondorskaya & Shebalin* [1977] list a destructive earthquake that happened in 1807 with a magnitude of ~6.7 and cited *Gorshkov* [1947] and *Mushketov & Orlov* [1893] for this event. The epicentre is said to be beneath Almaty and they report “Terrible catastrophe in Almata”, but no further information is available.

Fault scarps with cumulative heights of 50 m and higher are abundant along the Almaty rangefront as a result of the Quaternary shortening and uplift. However, apart from one scarp

mapped by *Tibaldi et al.* [1997] near Almaty, no Holocene fault scarps, surface ruptures, recent deformation features, or other indicators for recent strong earthquakes have been documented along the northern Zailisky Alatau in the international literature. Also, with the exception of the easternmost section of the range near Chilik [*Selander et al.*, 2012], no slip rate of the rangefront fault has been published.

The geographical setting of Almaty is somewhat similar to that of Bishkek, the capital of neighbouring Kyrgyzstan, with both positioned at the foot of sub-ranges of the northern Tien Shan (Fig. 1b) mountain front. Bishkek, however, is located on the footwall of a thrust fault that uplifted Neogene units in the Quaternary to an intermediate elevation between the high ranges and the foreland. Abundant evidence for Holocene faulting can be found there. Fault scarps that offset alluvial fans by ≥2m are present, and palaeoseismological trenches across the frontal Issyk-Ata Fault reveal evidence of at least two surface-rupturing earthquakes in the past ~10,000 years [*Landgraf et al.*, 2016]. *Thompson* [2001] reports four surface-rupturing events since the last glacial maximum (LGM) from the rangefront and *Smekalin et al.* [2016] identified an earthquake that happened ~3,000 BP. These findings illustrate that Bishkek, with its ~850,000 inhabitants, is built along an active fault that has ruptured in earthquakes of M>7 in the past and will do so again in the future. Although Bishkek can suffer from the far-field effects of distant M~8 earthquakes like the 1889 Chilik and 1911 Chon-Kemin events, smaller local events may have the potential to be even more devastating due to the elevated proximal ground motion in the near-field.

Given the along-strike evidence of faulting and the overall shortening across the region, the absence of published mapped evidence for Holocene activity on the range-front adjacent to Almaty is curious, as the 250 km-long, minimally embayed range has impressive relief with up to 5,000 m high mountains overlooking the <900 m Kazakh platform. There is clear evidence that vertical tectonic motion has been localized here since the uplift of this part of

the Tien Shan in the Neogene [*Avouac et al.*, 1993; *Abdrakhmatov et al.*, 2016]. We investigate three possibilities to explain the previous absence of recorded activity: (i) The rangefront is indeed seismically inactive and during or before the Holocene, deformation migrated elsewhere. Earthquakes like the 1887 Verny event occur on faults in the higher parts of the Zailisky Alatau where traces of active faulting are subject to fast erosion and/or difficult to identify, or they occur buried within the Kazakh platform without clear surface expression. (ii) The rangefront is seismically active, but the recurrence intervals of large events are so long that any morphological evidence has been obliterated by erosion and sedimentation. (iii) The rangefront is seismically active and geomorphological evidence for past surface-rupturing earthquakes does exist, but has been overlooked thus far.

In this paper we review all available evidence for active faulting along the Zailisky Alatau. The geomorphological evidence for active tectonics is investigated at eleven different sites (labelled S1-S11 from west to east) along the northern front of the Zailisky Alatau. We cover a ~250 km long section of the rangefront centred on Almaty (Fig. 2a) using field observations, remote sensing, and dating of Late Quaternary deformation. We document clear evidence for surface rupturing earthquakes since the LGM, and provide the first estimate of a slip-rate on the fault based on Quaternary dating of measured offsets. Finally, we put our morphologic observations of the Almaty rangefront into the wider regional context to explore implications for the tectonic evolution and seismic hazard of the Tien Shan.

2. Methods

We applied a wide set of methods to detect and document morphological evidence of active tectonics, including remote sensing, photogrammetric techniques, differential GPS profiles, field mapping, and Quaternary dating.

2.1. Satellite imagery and DEMs

SRTM1 elevation data and the ALOS JAXA DEM were used to produce slope, hillshade, aspect, and terrain ruggedness index (TRI) maps of the Zailisky Alatau with QGIS [*QGIS Development Team*, 2017]. The TRI is a measure for the difference in elevation between a raster cell and its neighbouring cells [*Riley et al.*, 1999]. It reveals landscape features characterized by changes in slope and with high relief, such as areas of uplift by faulting or river incision. These data allow us to observe large-scale features of tectonic geomorphology over wide areas as they have a ground resolution of 30 x 30 m. To overcome the issue of the relatively low resolution of these global datasets, we acquired SPOT6 stereo satellite imagery of a narrow strip along parts of the rangefront. This dataset has a ground resolution of 1.5 m and we produced a digital elevation model (DEM) with 3 m ground resolution using commercial software (ERDAS IMAGINE).

Optical satellite images were used to identify fault scarps and lineaments. We analysed recent and past Google Earth imagery (1984-2017; Digital Globe - Landsat/Copernicus, Cnes/SPOT), the SPOT6 data, and declassified Corona satellite imagery (~2 m resolution) from the 1960s. The latter has the advantage of covering a time at which some tectonic features were not yet obliterated by urban development and infrastructure projects [*Mackenzie et al.*, 2016].

2.2. Field-based drone DEMs

We produced high-resolution DEMs from aerial images collected from an unmanned aerial vehicle (UAV, drone) to analyse the geomorphological setting of several sites in detail. A DJI Phantom 2 quad-copter was used to carry a Canon PowerShot SX230 HS compact camera with internal GPS receiver to take hundreds of overlapping images from up to 50 m altitude. Commercial software (AgiSoft Photoscan) was used to produce a point cloud and a DEM with the Structure-from-Motion method (SfM) [e.g., *Bemis et al.*, 2014]. Ground control

points for reference were located with differential GPS (DGPS). Further details of our survey and processing steps are reported in Abdrakhmatov et al., 2016. The resolution of the DEMs is on the order of 0.1 m and they typically cover areas of 0.2-0.5 km². As with the satellite data, we computed slope and hillshade maps to visualize the deformation features. The DEMs will be made available through OpenTopography (www.opentopography.org).

2.3. Offsets measurements at scarps

We measured the vertical offsets of planar geomorphic markers such as alluvial fans and river terraces. Elevation profiles and swaths were extracted using QGIS algorithms. We used swath profiles for the SRTM1-based elevation data to show the larger-scale topography. The drone-DEMs and the SPOT6-DEM were analysed using narrow single-track profiles in order to make use of the very high resolution. By fitting straight lines to the profile segments above and below the scarps, respectively, the vertical offset at the fault scarps was calculated using linear regression and the vertical separation between the two fitted lines at the steepest part of the scarp. In the case of surfaces that have the same dip both in the hanging wall and in the footwall of the fault, the along-profile location of the fault surface projection does not influence the measured vertical offsets. However, when the dips on either side of the fault do vary, the selection of fault location affects the result of the estimated offset based upon the elevation measurements. For most sites analysed here, we do not know the exact location of the fault projection to the surface from outcrops. In these cases, the position of the fault was defined at the location of the maximum slope angle of the scarp. Surveys of the present-day stream beds showed that the post-depositional tilt of the fitted surfaces is negligible. The geometrical error introduced by the landform geometry in the sense of *Mackenzie & Elliott* [2017] also does not affect our results significantly beyond the noted 10% uncertainties.

Uncertainty in the precise fault location is difficult to quantify without independent information, for example, from paleoseismological trenching or outcrop studies. Further

errors stem from the vertical resolution of the DEMs and the non-planar behaviour of the upper and lower fan surfaces used to estimate the offset. The SRTM1 data have a vertical accuracy and resolution of a few meters [*Smith & Sandwell*, 2003], but it is impossible to quantify the relative accuracy of nearby point positions across the fault. We estimate the resolution of the SPOT DEM to be down to 3 m under favourable conditions, but less than that in areas with steep slopes. The drone DEMs have an error of less than 0.5 m, which comes from the image quality, the photo matching process, and the uncertainty in the DGPS locations of the ground control points, which is <0.1 m. We expect the combined error of the vertical offsets measured for this study to be around 10%, but we assign at least ±1m error for each offset to factor in the uncertainties related to the geological setting, choice of profile location, etc. The purpose of this paper is mainly to document a variety of morphological evidence for active faulting along the Almaty rangefront. With the exception of one site, we do not measure slip rates for which a more in-depth calculation of the offset errors would be required. We thus report the measured offsets without the errors in the following, and we emphasize that we present first-order observations that allow us to draw a general picture of the regional tectonics.

At two of our sites we used real-time kinematic (RTK) DGPS profiles instead of elevation data extracted from the DEMs to measure the offset of river terraces. Thus, the error is reduced to the uncertainty of the DGPS measurements (<0.1 m) and the location of the fault along profile. Specific details of the measurements made at individual sites are described in the appropriate site description.

2.4. Radiocarbon dating

Radiocarbon dating at site S7 was performed on charcoal and charcoal-bearing bulk sediment samples in silty layers. The samples were sent to BETA Analytic Inc. (Miami, FL, USA) for

AMS radiocarbon dating. Standard acid/alkali/acid or acid wash pre-treatment was applied to the samples and INTCAL13 [*Reimer et al.*, 2013] was used for calibration.

3. Geology, tectonic setting, and geomorphology

3.1. Geological background

The Tien Shan is an E-W trending mountain belt that has formed due to the collision of India and Eurasia in the Cenozoic. The mountain range is located more than 1,000 km north of the actual plate boundary delineated by the Himalaya, but GPS studies show that ~12 mm/a of the total N-S shortening is taken up in the eastern Tien Shan and ~20 mm/a in the western part—a sizeable portion of the overall India-Eurasia convergence [*Abdrakhmatov et al.*, 1996; *Zubovich et al.*, 2010]. This E-W gradient in the rate of shortening is due to the clockwise rotation of the relatively rigid Tarim Basin, bounding the Tien Shan to the south, about an Euler pole located near the eastern end of the Tien Shan range [*Avouac et al.*, 1993]. GPS data also reveal a component of left-lateral shear in the area between Lake Issyk Kul and the stable Kazakh platform. Relatively large spacing and uncertainties in the GPS velocities of *Zubovich et al.* [2010] do not permit the discrimination of active faulting located precisely at the rangefront [*England & Molnar*, 2015].

Continental crustal growth took place by the accretion of a large subduction-accretion complex during the Palaeozoic [*Burtman*, 1975; *Windley et al.*, 1990]. These rocks now form the basement of the Tien Shan. In the Mesozoic and the early Cenozoic, tectonic quiescence led to the creation of a vast erosional surface or peneplain [*Goryachev*, 1959; *Makarov*, 1977; *Burbank et al.*, 1999]. While the uplift of parts of the Tien Shan started before the Neogene, the latest phase of uplift in the Northern Tien Shan piedmonts has been ongoing since the Late Miocene [*Bullen et al.*, 2003; *Sobel et al.*, 2006]. The erosional surface has been uplifted in the most recent phase of mountain growth and is preserved in many parts of the Tien Shan as

213 a convenient marker for differential uplift [*Sobel et al.*, 2006; *Oskin & Burbank*, 2007] (Fig.
214 3). The fact that the peneplain is so well preserved in many places indicates rather rapid uplift
215 throughout the mountain range [*Buslov et al.*, 2008]. Uplift has occurred along ~E-W trending
216 thick-skinned reverse faults as evidenced by uplifted basement complexes [e.g.,
217 *Abdrakhmatov et al.*, 2001]. The basement along the rangefront mainly consist of
218 Carboniferous-Permian series and granitic, granodioritic, and dioritic intrusives [*Nalivkin*,
219 1983].

220 North and south of the Tien Shan, flexural foreland basins contain up to several kilometers of
221 sediment (see *Avouac et al.* [1993] and references therein). For example, the Kashi Basin in
222 the Western Tarim is filled with 6-10 km of Neogene sediment [*Sobel et al.*, 2006]. The high
223 ranges alternate with ~E-W elongated intermontane and intramontane basins filled with
224 Cenozoic deposits as a result of increased erosion during mountain building. These basins
225 record active tectonic deformation along the mountain fronts, but also highlight deformation
226 away from the ranges toward the basin centres in the form of folds and fault scarps in alluvial
227 fan and fluvial terrace sequences [e.g., *Brown et al.*, 1998; *Abdrakhmatov et al.*, 2002;
228 *Thompson et al.*, 2002].

229 Glacial advances in the Tien Shan do not strictly coincide with the global LGM [*Zech*, 2012;
230 *Takeuchi et al.*, 2014]. Glacial advances during the last glacial cycle were probably at their
231 maximum around marine isotopic stage (MIS) 4 (~60-70 ka), but younger moraines are also
232 preserved [*Zech*, 2012]. For example, *Koppes et al*. [2008] report regional advances during
233 MIS 3, and document locally preserved MIS 2 remains near modern glaciers. The sparse
234 dataset available makes it difficult to identify those glacial advances that left a major impact
235 in the landscape in the form of alluvial fan series or river terraces. Therefore, we use the term
236 LGM here in the sense of the global LGM around 26-19 ka [*Clark et al.*, 2009]. A regional
237 correlation of river terraces has been established in the Tien Shan based on morphological

arguments [*Thompson et al.*, 2002 and references therein; *Burgette et al.*, 2017]. Four main terraces QI-QIV represent, respectively, early Pleistocene, middle Pleistocene, late Pleistocene, and Holocene stages of terrace formation, and may again be subdivided into several substages. Although the local terrace systems may differ from the observed regional pattern, some main features seem to be characteristic for Tien Shan terraces in general. In the absence of Quaternary dating, those terraces may be used to estimate the approximate age of geomorphic markers.

3.2. Tectonic setting and seismicity

Instrumental seismicity in the Tien Shan is high compared to the forelands, with greater activity along its southern boundary and at the contact between the Tien Shan and the Pamir (Fig. 1). Earthquakes in the Tien Shan typically have depths of 15-30 km. Deeper events are mainly recorded in the forelands. In the area of the Zailisky Alatau, only a few earthquakes for which moment tensor solutions could be determined from teleseismic waveform analyses occurred in the instrumental period [*Sloan et al.*, 2011]. These events have mostly reverse mechanisms, although some occurred on strike-slip faults. In general, instrumental earthquakes in the study area cannot be ascribed individual faults due to the lack of surface breaks and the abundance of possible seismogenic structures. Furthermore, the location errors are high compared to the spacing of mapped active faults. Moderate instrumental seismicity and microseismicity are well documented for Almaty and the surrounding regions [*Torizin et al.*, 2009; *Mikhailova et al.*, 2015]. The historical record reaches back only a few hundred years, but includes two of the strongest continental earthquakes on record. Both the 1889 Chilik and the 1911 Chon-Kemin earthquake had magnitudes of M~8 and produced significant surface ruptures. No surface ruptures were reported for the 1887 M~7.3 Verny Earthquake, and it remains unknown whether it occurred on the rangefront fault or in the mountains (Fig. 1b). Palaeoseismological data on earthquakes are available from the Issyk-

Ata Fault south of Bishkek [*Thompson*, 2001; *Landgraf et al.*, 2016], from the Toraigyr Fault east of Almaty [*Grützner et al.*, 2017], and from the northern shores of Lake Issyk-Kul [e.g., *Korjenkov et al.*, 2006, 2007, 2011]. These data show that faults tend to break in large earthquakes, but have recurrence intervals of several thousand years. These long intervals can lead to a near-complete obliteration of the surface expression of active faulting in between two successive events [*Grützner et al.*, 2017]. Another major issue for the preservation of fault scarps and other tectonic features is burial beneath the abundant loess cover in the piedmonts [*Fitzsimmons et al.*, 2016].

A large number of active faults, especially in the Almaty area, are published on geological maps. Oscillating differential vertical motion in Almaty of up to 5 mm/a across faults was reported by *Atrushkevitch et al.* [1988] based on geodetic measurements made across a levelling network. The authors speculate on a relation with moderate to strong earthquakes that occurred up to 200 km away elsewhere in the Tien Shan, for which the observed vertical motion could serve as a precursor. However, no nearby strong earthquakes occurred in the observation period that could be tied to tectonic motion along those faults. Non-tectonic causes like groundwater charge and discharge are known to produce differential motion along faults [e.g., *Cuenca et al.*, 2013] and several other factors might lead to similar patterns of surface deformation. *Tibaldi et al.* [1997] report a 2-20 m high scarp east of Almaty and interpret it as the surface expression of a SW-NE striking fault-propagation fold. Unfortunately, this feature coincides with the terrace risers of the Small Almatinka River (Малая Алматинка) and thus its usefulness as a geomorphic marker for fault activity may be compromised.

3.3. Morphology of the Zailisky Alatau rangefront

The ENE trending Zailisky Alatau (Figs. 1, 2a) is the northernmost range of the Tien Shan between 75°-78.5° E. It reaches an elevation of almost 5,000 m above sea level (Pik Talgar near Almaty, Fig. 4). The Chon Kemin valley separates the Zailisky Alatau from the Kungey Range in the south. The Kazakh platform north of the Zailisky Alatau has an elevation of 900-1,000 m near the rangefront and gently decreases in elevation further north. The highest parts of the Zailisky Alatau have rather flat tops with deeply incised valleys in between them, indicating that the elevated Mesozoic peneplain still controls the morphology. Between the foreland and the highest peaks, pronounced north dipping surfaces with little relief mark the uplifted remnants of the Mesozoic peneplain (Figs. 2-4). The morphology suggests that these intermediate-height peneplain surfaces are bounded by reverse faults on both sides.

Large parts of the rangefront are covered in thick loess deposits (Fig. 4). Loess is found between ~750-2,400 m elevation, with the thickest deposits in the foothills of the Northern Tien Shan occurring around 1,000-1,300 m [*Machalett et al.*, 2006]. In the central part of the mountain range near Almaty (at Remisovka) [*Fitzsimmons et al.*, 2016], the loess sequence is ~80 m thick. It thins towards the east and towards the west. The middle of the loess section is late Pleistocene in age [*Machalett et al.*, 2006], but the last two peaks in loess deposition occurred around MIS 3 and during the LGM. These depositional periods left layers of ~8 meters thickness [*Fitzsimmons et al.*, 2016].

The loess-covered foothills of the range exhibit fault scarps with heights of 50 – 100 m (Figs. 3, 4). These scarps are abundant and can be found almost everywhere along the Zailisky Alatau. The thickness of the loess cover and the underlying bedrock morphology are mostly unknown, thus hampering any attempts to measure fault slip rates at the rangefront.

4. Active tectonics along the rangefront

In this section we discuss the study sites S1-S11 in detail (Table 1). We work our way from west to east and report on morphological indicators of active faulting.

4.1. Western Zailisky Alatau

The Almaty rangefront fault intersects, in the west, the Dzhalair-Naiman Fault, a long NW-SE trending strike-slip structure that extends into the Kazakh platform (Figs. 2, 5). The range reaches an elevation of approximately 2,500 m here. An isolated plateau north of the rangefront, with elevations between 1,000-1,400 m, dips gently to the north between the latitudes 75.5°-76°E. Incised streams (Figs. 2, 5) and a sharp drop in elevation indicate uplift along an ENE oriented, S-dipping reverse fault (Fig. 5). Basement rocks crop out in the hanging wall that sits about 150-400 m above the undeformed platform. The relief fades out towards the eastern end of the plateau, but gentle hills and incised streams can be identified as far as Almaty (Fig. 2). These features indicate large-scale uplift that probably started relatively recently because the streams incise into the foreland sediments. The entire western part of the piedmont is covered by a layer of loess with varying thickness.

4.1.1. Akterek (S1, S2)

Near the village of Akterek (russ. Актерек) the rangefront fault has uplifted the plateau surface described above. Basement rocks crop out in the hanging wall; a thin Cenozoic basin section is still preserved and crops out in the hanging wall. Topographic throw is up to 400 m. The rangefront fault turns to the NW at its western end. A number of small streams, some of them intermittent or ephemeral, drain the plateau to the north (Fig. 5a). River Zhamanty (russ. Жаманты) is the largest perennial stream and has incised deeply into the uplifted plateau surface. It leaves the mountainfront at our study site S2. Different generations of alluvial fans can be distinguished based on their surface roughness, but none have been dated so far. Distinguishing by their elevation, modern day stream courses, and the degree of fan

dissection, we grouped them into T1-T4 (youngest to oldest, Fig. 5d). We expect the fan surfaces to be Late Quaternary in age, the youngest ones probably post-dating the LGM (see also *Thompson et al.* [2002] and *Burgette et al.* [2017], and the references therein for Quaternary terrace sequences in the Tien Shan). Burial mounds (kurgans) are found on alluvial fans of all generations. These kurgans are probably not more recent than Iron Age (8th-4th Century BC) [*Hall*, 1997; *Sala & Deom*, 2005], which can thus be seen as a minimum age of the alluvial surfaces. A loess layer of varying thickness is present on top of all alluvial surfaces. All alluvial surfaces are truncated at the rangefront, and thus interpreted to be vertically offset by the rangefront fault.

We observed N-facing fault scarps (Fig. 5) that offset at least three generations of alluvial fan surfaces T2-T4 except the modern river beds T1. The western section is oriented W(NW)-E(SE) and joins the NW-trending fault. The scarps in the east are sub-parallel to the strike of the rangefront fault and strike NE. All scarps are degraded and no fresh surface breaks were observed. We analysed two high-resolution drone DEMs that capture the scarp at S1 and S2, respectively.

At study site S1, the offset can be traced for ~2 km in the T3 and T4 surfaces. We observe a relatively uniform throw of 2.2-2.5 m (Fig. 6a, b). Note that we only show two representative profiles here. The scarp is located ~1.5 km north of the main topographic step. Judging by the degradation of the scarp and comparison with studies from other sites in the region [*Thompson et al.*, 2002; *Landgraf et al.*, 2016; *Grützner et al.*, 2017], we suspect that one or more Holocene earthquakes caused the offset.

Study site S2 is located further NE along the same scarp system at the mouth of River Zhamanty. Fan surfaces T3 and T4 contain abundant kurgans. T4 is dissected by ephemeral streams that have incised into the alluvium. We have no direct age control of T4 but its morphology suggests that it is much older than T2 and T3, though probably Late Pleistocene

based on similar morphology of dated surfaces elsewhere in the Northern Tien Shan (Thompson, 2001; Thompson et al., 2002; Burgette et al., 2017). The fault scarp is degraded at site S2 relative to S1, but continuous for ~1.5 km. It forms the NE continuation of the scarp at site S1 and lies ~500 m away from the main topographic step. Vertical throw on T4 is ~7 m with a smaller scarp of ~1 m height present further downslope (Fig. 6c). A second nearby profile across the T4 fan surface identifies a throw of 6 m. This offset was found at the contact of two different fan generations (Fig. 5d). The scarp heights at S2 are similar within their error bounds, but consistently higher than at S1. This variation in height may indicate that the topographic step was formed by multiple earthquakes. Based on the morphology and the scarp heights at sites S1 and S2, we suggest that the offset of T3 represents the most recent surface rupturing earthquake(s), which probably did not occur in the past few hundred years, but likely after the LGM. T4 has recorded multiple events based on its scarps being several times the height of T2 and T3 scarps.

4.1.2. Fabrichny (S3)

Site S3 lies at the piedmont south of the town of Kargaly (russ. Каргалы), the former Fabrichny (russ. Фабричный). A small perennial stream exits the mountains here and incises deeply into the loess that covers the mountain front. These hills show a sharp break in slope (black arrows in Fig. 7a). The morphology of the landform suggests that this is a fan, with sediment composed of loess reworked from higher elevations in the catchment. The stream has a small catchment that only encompasses the degraded mountain slope below the peneplain surface (~900 m above the Kazakh platform; Fig. 2a). As the stream incises into the loess cover, mass wasting processes dominate the sediment supply in large parts of the catchment. The loess has an unknown thickness, as outcrops observed in nearby river banks do not expose any other material.

At least four kurgans can be identified on the alluvial surface in declassified Corona satellite imagery from 1969 (Fig. 7a). Those burial mounds are not likely to be younger than Iron Age [*Sala & Deom*, 2005]. Currently the archaeological remains are less visible because the site is being developed for private housing. We found a N-facing, ~1 m high fault scarp that offsets the youngest alluvium (white arrows in Fig. 7b). The scarp runs ENE for at least 700 m, is marked by a gentle break in slope, and has a rather uniform height. Due to the housing project, the scarp is more visible in 1960s Corona satellite images than in modern imagery (Fig. 7a). We interpret the scarp as the surface expression of the most recent surface-rupturing earthquake(s). The scarp morphology suggests that the offset was produced after the LGM, probably several hundreds or thousands of years ago. Fabrichny is located in the epicentral area of the 1887 Verny Earthquake (M7.3) that is not known to have ruptured the surface. However, it remains unclear whether the 1887 earthquake ruptured the fault we investigated but did not reach the surface, or if it occurred on some unknown fault in the mountains.

4.2. Central Zailisky Alatau

The central part of the Zailisky Alatau is characterized by higher elevations of 3,000-4,000 m west of Almaty. Further east even higher elevations are present and the almost 5,000 m high peak Talgar 30 km SE of Almaty is the highest in the range (Fig. 4). The peneplain surface is well-preserved in this part of the Alatau (Fig. 2). It has a width of approximately 5 km and is tilted towards the north. The peneplain occupies an altitude range of 2,000 – 2,500 m in the western part and lowers to a range of 1,200-1,800 m in the eastern parts near Almaty, where it disappears. Further east, a few patches of peneplain-like plateaus can be found between the high Zailisky Alatau and the Kazakh platform, but in general they are more heavily eroded, have a higher internal relief, and are less continuous than in the west.

Within the peneplain, ENE striking scarps near Ushkonyr are obvious in satellite imagery and in the digital elevation model (DEM; Figs. 2c, 3). These scarps face SSE, have a height of

several meters, and are up to 10 km long. North of the scarps, incision of the streams testifies to uplift, while south of the scarp only relatively minor incision is evident. This is consistent with decreased stream power due to the aggradation of sediment against the scarp. These lineaments are interpreted as backthrust faults since they are parallel to the mountain front and to the main strike of the ridge, which suggests that they are structurally related to the uplift.

4.2.1. Almaty (S4)

Almaty is mainly built on the alluvial fans of four rivers that drain the Zailisky Alatau, and increasingly occupies the loess covered foothills in the south (Figs. 4, 9). This urban development makes it difficult to identify any geomorphological indicators for active faulting. The main roads in Almaty run in a system orthogonal to the drainage directions. Since the roads are relatively wide they are good targets to measure topographic profiles along them. Along one of the N-S running main roads, Ul. Furmanova, we observed in the field a break in slope just north of the intersection with the E-W running Ul. Satpayeva (N 43.239927°; E 76.948643°). This feature is also visible in digital topography (Profile P2 in Fig. 9a, b).

In order to test whether or not this is a north-facing scarp of tectonic origin, we analysed the freely available SRTM1 (NASA) and ALOS (JAXA) topographic datasets. In the JAXA DEM hillshade map, it is clear that the break in slope is a linear feature that can be traced across the alluvial fan (Fig. 9a). To measure the offset across the scarp, we extracted the elevation data along three N-S running main roads: Ul. Seyfullina (P1), Ul. Furmanova (P2), and Ul. Dostyk (P3; from west to east in Fig. 9).

The scarp in P1 cannot be identified in the SRTM1 data (Fig. 9c), but is just visible in the JAXA DEM (Fig. 9d). Neither SRTM1 nor the JAXA DEM can reveal the scarp in P2 (Fig. 9g, h) and P3 (appendix A). The relatively poor resolution of the datasets (~30 x 30 m) is not suitable to resolve such tectonic features in an urban environment, even if it can be recognized on a hillshade map.

To overcome the issue of the low resolution we acquired SPOT6 stereo satellite imagery and extracted the elevation data of the same three profiles P1-P3. Although we centred the profiles on the middle of the wide Almaty streets, the data show spikes (Fig. 9e, i; appendix A). This is most likely caused by the nearby multi-storey buildings and trees. However, straight lines fitted to the profiles on either side of the scarp location, as identified in the field and in the JAXA DEM, reveal a significant vertical offset. In profile 1, the vertical offset is ~5 m (Fig. 9f), whereas it is ~7 m in profile 2 (Fig. 9j). No offset was detected in profile 3 (appendix A). We interpret the feature as the surface expression of active reverse faulting for two reasons: (i) The scarp clearly offsets the entire alluvial fan and is visible in two profiles more than 1 km apart. This rules out local building ground modifications or other anthropogenic cause. (ii) The scarp aligns with the main mountain front on either side. A more detailed morphological investigation of the scarp in the field is impossible since it is located in the heart of the city.

On a wider scale, the drainage pattern indicates a broad region of uplift of the foreland sediments west of Almaty. We find an arched/warped surface into which streams and rivers incise (Fig. 8). The uplift manifests in the field only as gently sloping hills, but it is clearly discernible in the slope map. In addition to this general pattern in the west and northwest of Almaty, there are narrower anticlinal structures with NE trends in the northern outskirts of the city (Fig. 8). We observe pronounced incision into the foreland sediments here. The river banks are almost vertical walls of several meters height. Individual anticlines can be distinguished and the general morphology indicates rather recent uplift. This structure implied deformation above a thrust fault which must underlie the city. In the platform northeast of Almaty, there are no topographical signatures of active tectonics. However, *Macklin et al.* [2015] report deformed fine grained glaciofluvial deposits of post-LGM age (Fig. 8b) near Kosmos. Radiocarbon dating of an organic-rich layer yielded an age of 17.1 ± 0.22 ka cal BC. These layers are folded on a 1 m scale. They are not likely to represent liquefaction structures

because the deformation is only found here and is not widespread in these layers. Similarly, we rule out glacial deformation features or a slump: the slope is very shallow—the layers are almost horizontal—and the deformation is localized. We interpret the deformed layers as indicative of compression caused by a small-scale fault-propagation fold on top of a thrust fault that takes up shortening in the foreland. The fact that no deformation is detectable in the 30-m DEM would confirm the observation made elsewhere that the recurrence intervals of large, surface rupturing earthquakes are typically long and that surface deformation features are rapidly obliterated by sedimentary processes. In this case, the deformed layers were found in a reach of the Talgar River that drains a large catchment of the Zailisky Alatau and has a high sediment load.

4.2.2. Talgar (S5)

The Talgar River drains the highest peaks of the Zailisky Alatau and is fed by a number of glaciers. A dam is located 1 km upstream of the mountain front to mitigate floods and mudslides. To the west and east of the river, small remnants of the peneplain are possibly preserved, although they are intensely incised. The city of Talgar (russ. Талгар) is built on the alluvial fan of the Talgar River and has, similar to Almaty, seen a recent spike in urban development. Due to the presence of the city, it is not clear if there are different generations of alluvial surfaces here. The foothills behind the city form 100 – 300 m high, relatively steep fronts and are covered in loess of unknown thickness. Exposures within recent landslides observed in the field constrain that the loess exceeds 20 meters thickness. Between Almaty and Talgar, housing projects have started to develop those loess covered foothills. East of the mouth of the river, a relatively smooth surface surrounded by higher mountains is tilted toward the west (Figs. 8, 10).

We did not observe any fault scarps cutting the Talgar alluvial fan during our field survey. In order to check if there is large-scale evidence of active tectonic deformation preserved in the

484 landscape, we analysed the SRTM1 and JAXA ALOS DEMs (Fig. 10) after our field work.
485 We calculated elevation, slope and TRI maps of both datasets and identified lineaments that
486 cross the alluvial fan at high angle to the drainage direction. These lineaments align with the
487 mountain front in the west and the northern edge of the smooth plain in the east (arrows in
488 Fig. 10a; for a clearer view the arrows were left out in Fig. 10b).

489 Elevation data were extracted along two profiles P4 and P5 and processed as described in
490 section 2. The profiles run parallel to the drainage direction in order to avoid crossing
491 different fan generations. Profile P4 does not reveal a sharp break in slope at the location of
492 the scarp. Instead we observe a broad zone of folding with a wavelength of ~1 km. (Fig. 10c-
493 f). This structure can be identified in both the SRTM1 and the JAXA DEMs. The surface of
494 this anticline deviates up to ~5 m from a straight line fitted to the upslope and downslope
495 sections on either side of the fold. The section uphill of the fold in profile P4 is also
496 systematically offset with respect to the section downstream of the fold.

497 Profile P5 exhibits a change in slope angle where we identified the lineament in the slope map
498 (Fig. 10g-j). We observe ~6 m vertical offset in the SRTM1 data (Fig. 10g, h) and ~5 m
499 vertical offset in the JAXA DEM. It is not clear whether this feature is a highly degraded fault
500 scarp, i.e. an ancient surface rupture, or related to a monocline/anticline structure above a
501 blind fault. The presence of the anticlinal structure in P4 makes it likely that P5 also records
502 blind faulting. Such features can hardly be seen with the naked eye or in imagery, but are
503 clearly expressed in topographic data.

504 The observed folding in the Talgar fan is interpreted as the surface expression of a blind thrust
505 fault that caused a fault-propagation fold in the overlying sediments. We cannot assign an age
506 to the structures, but suspect them to be several thousand years old. The lack of any more
507 distinct tectonic landforms may be explained by the prevalence of loess that accumulates

against the piedmont and/or by a period of relative tectonic quiescence. We cannot distinguish between these two alternatives without further investigation.

4.2.3. Rahat (S6)

Rahat (russ. Рахат) is a settlement that is situated at the mouth of a perennial stream that occupies a rather wide and linear valley. An alluvial fan formed at the base of the mountain front the western half of which is occupied by the village. The foothills south of Rahat are covered in loess and reach up to 500 m above the elevation of the Kazakh platform, with an ~50 m high scarp in the loess-covered hills marking the northernmost edge of the mountain front (Fig. 11).

At our study site the mountain front is embayed to the south and occupied by a flat-bottom valley of a north-draining catchment from the Zailisky Alatau (Fig. 11b). At the western edge of the valley, we find a loess-covered surface which forms the oldest of a series of river terraces (T4). The T4 terrace surface has been modified, with the construction of an earth mound surrounded by two square ditches. The age of this archaeological site, and the terrace on which it sits, are unknown as far as we know. The east flank of the valley is occupied by a cemetery situated on a lower terrace level T3 (Fig. 11c). The same terrace is also preserved as a narrow strip along the western river bank. Apart from the present-day river bed T1, we identified another river terrace T2 (Fig. 11c) in the centre of the valley.

A fault scarp in different stages of degradation is visible in the field (Figs. 11, 12). The entire lower part of valley was and still is subject to anthropogenic interference. Channels and weirs have been built for irrigation and various dirt roads wind around excavated material. These features make it difficult to properly assess the scarp height. We therefore produced a DEM from drone imagery with the methods described in section 2. The DEM has a resolution of ~0.1 m. Despite the complicated surface conditions the scarp is visible as a continuous feature across the valley, except in the modern stream beds.

We extracted the elevation along four profiles from different terrace surfaces in the valley (Fig. 11b, c). Profiles 1 and 3 show ~5 m offset across the scarp. These profiles are situated on the lowest (= youngest) surface that is affected by the offset, T2. Profile 2 is from the modern river bed T1 and exhibits neither a scarp nor a retreated knickpoint in this surface (Fig. 11c). The highest (= oldest) terrace level that we investigated, T3, is offset at two locations (profile 4). At 130 m profile distance, we observe 3.5 m of vertical offset. Another 11 m of vertical offset was found at the northern end of the profile at a loess quarry. The shape of the scarp is anthropogenically modified, but the total vertical throw of 11 m is measured between adjacent intact fluvial surfaces.

We interpret the scarp to be caused by thrust faulting in past earthquakes. It is impossible to distinguish between single-event and multi-event scarps due to the poor state of preservation (Figs. 11, 12). Past reverse faulting earthquakes in the Tien Shan have produced offsets of more than 5 m [e.g., *Abdrakhmatov et al.*, 2016], but it is not clear whether the lower scarp can be assigned to a single event. The difference in the vertical offsets of different fluvial terraces (i.e., between the two profiles 1 and 3 and profile 4) indicates that more than one earthquake is recorded in the landscape. The older (= higher) terrace surface T3 was probably uplifted by at least one additional event compared to the lower terrace T2.Neither of these surfaces have been dated, but the state of preservation indicates that the surface ruptures probably happened after the LGM, likely in the Holocene.

4.3. Eastern Zailisky Alatau

East of 77.5°E, the Zailisky Alatau reaches elevations of less than 3,000 m. The rangefront is sinuous here and curves around the rather wide valleys carved by the main rivers. Straight mountain fronts are often interpreted as tectonically active, while sinuous ones tend to indicate lower grades of tectonic activity or inactivity [*Bull & McFadden*, 1977]. A possible alternative explanation for this observation is the higher discharge of the main rivers

558 compared to those in the central and western sections of the rangefront. It is unclear if the
559 higher sinuosity of the rangefront is entirely due to a higher erosional power of the streams or
560 rather caused by lower uplift rates. The basement geology is not significantly different from
561 other parts of the rangefront, which makes it unlikely that lithological changes (less/more
562 resistant to erosion) can explain the observations. In the foreland north of the eastern section
563 there are no morphological hints that would clearly indicate uplift. Several parallel fault
564 strands can be identified in the easternmost parts of the mountain front (Fig. 13). Here,
565 *Selander et al.* [2012] report offset and deformed Q2 terraces giving tentative slip rates of
566 0.8±0.5 mm/a and 0.43±0.3 mm/a for the two parallel faults, respectively (Figs. 1b, 13).
567 While the offsets were measured in the field, no direct dating of the surfaces was performed.
568 An age of 100±30 ka was assumed based on data from Q2 terraces in other parts of the Tien
569 Shan dated by *Thompson et al.* [2002] and *Bowman et al.* [2004]. This slip rate, therefore, has
570 to be taken as an estimate because the ages were not verified by direct Quaternary dating,
571 although the assumptions are reasonable. In the east, the Zailisky Alatau diminishes in the Ili
572 Basin.

573 *4.3.1. Slip rate site near Chilik (S7)*

574 4.3.1.1. River terraces

575 Site S7 is located near Chilik (Russ. Шелек) at the mouth of a stream that crosses a plateau of
576 1,100-1,200 m elevation between the Zailisky Alatau and the Kazakh platform. Here the Big
577 Almaty Canal runs in front of the loess-covered foothills (Fig. 13). We found a series of four
578 river terraces preserved here (Figs. 14, 15). The oldest and uppermost terrace T4 forms the
579 flat top of a ~200 x 400 m wide hill at the right bank of the river. Terrace T3 is preserved as a
580 flat, elongated surface at the right bank of the stream and as an incised remnant at the left
581 bank. Terrace T2 is best preserved east of the stream, but an ~100 m long and 15 m wide
582 section is also seen on the west side. T1 is the modern stream bed. We interpreted those

583 terraces as geomorphological markers that would allow us to determine the vertical uplift rate
584 of the rangefront fault. This site is the best target for measuring a long-term slip rate that we
585 were able to find along the entire mountain front.

586 In order to determine the vertical offset across the fault and to correlate the terraces we
587 acquired a photogrammetric DEM with the method described above (Fig. 14). We also
588 measured profiles on top of the terrace surfaces with DGPS (coloured lines in Fig. 14). Due to
589 the nearby canal, the footwall profiles are much shorter than those on the hanging wall. The
590 steepest part of the fault scarp was set as the fault location and the vertical throw was
591 measured here. Since the terrace surfaces are almost exactly parallel to the present day river
592 bed, another choice (e.g., the base of the scarp or the centre) would not result in a significant
593 change in measured throw. We find a vertical offset of 50±1.3 m in terrace T4, and 30.4±1.6
594 m in terrace T3 on the east side of the stream (Figs. 15, 16).

595 Terrace T2 is offset 9.4±0.4 m on the east side of the stream (Fig. 16a), where it can be traced
596 both in the hanging wall and in the footwall. The terrace is offset by 14.4±0.6 m on the west
597 side of the stream compared to the present day stream bed (Fig. 16b). All errors are reported
598 as 2σ as calculated from the linear fit.

599 We conclude that the terraces have been consequently uplifted by the mountain front thrust
600 fault in multiple earthquakes. It is not possible to directly correlate the uplifted surfaces in the
601 hanging wall with their counterparts in the footwall, because any information on
602 sedimentation in the footwall is lacking. However, the absence of incision in the footwall and
603 the rather smooth surface indicate that deposition prevails here instead of erosion. Thus, the
604 amount of uplift must be taken as minimum value, although there was probably rather little
605 fluvial deposition adjacent to the present day mouth of the river. The thickness of the loess is
606 unknown here.

4.3.1.2. Radiocarbon dating

We dated terrace T2 to calculate the uplift rate (Table 2). The stratigraphy of terrace T2 is exposed in a 10 m high vertical wall carved by the stream (Fig. 17). The lowest part of the outcrop exhibits a 2 m thick layer of reddish medium to coarse gravels that dip 35° to the north (Fig. 17b). This dip angle is much steeper than that observed at the terrace surface and indicates that the gravels were tectonically tilted before terrace formation. An erosional unconformity marks the top of this unit. The gravels are overlain by an 8 m thick sequence of subhorizontal, layered coarse gravels with boulders in a silty matrix. These high-energy deposits indicate episodes of alluvial aggradation. A fine-grained unit of ~2 m thickness follows on top. These fine-grained sediments consist of several layers of silty material and fine-medium sands, corresponding to a phase of low-energy transport. Three of those fine grained layers contain numerous fragments of charcoal of up to a couple of millimeters in diameter. On top of the fine grained succession lies a ~2 m-thick layer of coarse gravels to boulders that is capped by a thin layer of loess (Fig. 17a).

We sampled the three fine-grained layers within the fluvial sequence at depths of 0.8 m, 0.95 m, and 1.7 m below the gravels, respectively (Fig. 17a). The uppermost sample (chilik-2016-upper) was a bulk sample with some charcoal in it and returned an age of 15,360-15,075 cal years BP. The samples from the middle layer (chilik-2016-middle) and from the lower layer (chilik-2016-lower) were pieces of charcoal and returned an age of 13,425 – 13,215 cal years BP and 13,735 – 13,115 cal years BP, respectively. Our uppermost sample is older than the lower ones which may be explained with reworking of the sediment before its final deposition at the current location. We have no direct constraints on possible inheritance of the samples, which would change the slip rates we calculate. However, we might expect that inheritance would not change our results substantially given the uncertainties and the age ranges of our samples. Since this is a bulk sample including fine grained sediment, the age is likely

somewhat overestimated. The gravel layer on top of the fine grained material indicates rapid deposition. We conclude that the terrace surface was abandoned not earlier than ~15 ka ago, and probably not much later than ~13.5 ka ago. In the following we use an age range of 13.3-15 ka for our slip rate calculations.

4.3.1.3. Slip rate

The age of terrace T2 and the corresponding measured vertical offset of ~14.5 m at the left bank of the river give an uplift rate of ~1-1.1 mm/a. The uncertainties in stratigraphic position of the samples and the error related to matching the footwall and the hanging wall across the fault do not justify calculating a more precise rate with propagating formal errors. We have no direct information on the dip of the fault, see discussion in section 5.1. A dip of 45° would result in a fault slip rate of ~1.4-1.6 mm/a. A shallower fault with a dip of only 30° would have a slip rate of 2-2.2 mm/a, a fault with a dip of 60° would yield a slip rate of 1.2-1.3 mm/a. The lowest terrace we encountered at site S7 has a vertical offset of 14 m at the left bank of the river (Fig. 16). This is much higher than the offsets observed elsewhere along the Almaty rangefront, for example at sites S1 and S2, and is also higher than the scarp found at Rahat (S6). The terrace has very likely been formed in multiple earthquake events. We conclude that the rangefront fault has a slip rate of between ~1.2-2.2 mm/a in this section, averaged over multiple earthquakes in the past ~13.3-15 ka and assuming dips of 30°-60°.

4.3.2. The Big Almaty Canal (S8)

The Big Almaty Canal (russ. Большой Алматинский канал; kaz. Үлкен Алматы каналы) is an irrigation canal that diverts water from the River Chilik further east to the Almaty metropolitan area where the water mainly serves agricultural and industrial needs. The canal was built in the late 1970s and contours around the front of the Zailisky Alatau for more than 150 km. From an engineering point of view, there are good reasons for choosing this location: the water is always available at an elevation higher than the crops, and close to the mountain

front, the canal can maintain a constant slope without having to circumnavigate the numerous alluvial fans. At some locations, the canal crosses streams and roads coming from the mountains. These crossings were realized with underground sections, tunnels, and aqueducts. Since construction of the canal required massive excavations, large stretches of the mountain front, where we suspect the rangefront fault to crop out, are now covered either by spoil or by the canal itself. Knowledge on past surface ruptures along the canal would not only help to understand the tectonic behaviour of the rangefront fault, but also be interesting from a seismic risk and infrastructure vulnerability point of view.

We analysed declassified Corona satellite imagery that were acquired in 1969 before the canal was built (Fig. 18). Along the rangefront we identified several spots in which faults scarps can clearly be seen in the grey-scale satellite photos. Most of these locations can also be found in modern Google Earth imagery. We found that the canal crosses the rangefront fault scarp several times. At study site S8, the canal was built directly on the scarp (arrows in Fig. 18) for a stretch a couple of hundred meters long. In this section the fault scarp appears as a very sharp line in smooth alluvial surfaces. Here it is much clearer in the imagery than in most other sites along the rangefront.

Unfortunately the canal deprives us of the opportunity to study these scarps in more detail, but the Corona imagery makes clear that the mountain front has been tectonically active in the past. No direct age control is available for this section of the fault, but the sharp morphological expression of the rupture leads us to conclude that it might be Holocene in age. We made our analysis of the Corona imagery after our field visit; future field work can aim to inspect the scarps and more detail and to evaluate their potential as paleoseismological trenching sites.

680 *4.3.3. East of Chilik (S9, S10, S11)*

681 In the easternmost part of the Zailisky Alatau, an ~10 km wide plateau with an elevation of
682 1,100-1,600 m separates the Kazakh platform from the highest parts of the mountain range
683 (Fig. 13). The plateau is formed of folded alluvial surfaces; river cuts expose folded Cenozoic
684 basin deposits. Abrupt breaks in slope mark both the northern and the southern boundary of
685 that plateau (Fig. 13). Around 78°E, a second fault strand parallel to the mountain front and
686 within the plateau becomes visible. This strand runs ~5 km S of the piedmont and is mainly
687 expressed as folded alluvial surfaces. Here, *Selander et al.* [2012] estimated fault slip rates of
688 0.8±0.5 mm/a and 0.43±0.3 mm/a for the frontal fault and the fault within the plateau,
689 respectively. These values are based on vertical offset measurements and ages of 100 ± 30 ka
690 are based on regional terrace correlation [cf. *Thompson et al.*, 2002]. We investigated three
691 sites S9-S11 near Chilik (Figs. 13, 19, 20).

692 4.3.3.1. Site S9

693 At S9 we observe three parallel faults that offset alluvial fans (Figs. 13, 19). The composition
694 of those alluvial fans and their stratigraphy are exposed in a river bank at S9 where a small
695 intermittent stream cuts into the scarp (Fig. 19b). We find mainly medium to coarse gravels
696 with a few finer-grained sandy units. The gravels are probably Pleistocene in age. In general,
697 the layers are sub-parallel with a few exceptions of internally deformed gravels on a meter-
698 scale. The fault itself does not crop out at S9. The general dip of the strata is 18° to the north.
699 This dip is much steeper than that of active alluvial fans anywhere near the rangefront, and
700 also steeper than the alluvial surfaces further south. We interpret these findings as evidence
701 for folding related to an underlying reverse fault, possibly a fault-propagation fold.

702 4.3.3.2. Site S10

703 Site S10 is situated at the mountain front ~12 km east of S9. A distinct fault scarp offsets
704 alluvial fans up to 1 km north of the main rangefront. The scarp can be traced for more than

7.5 km and is expressed in different generations of alluvial fans (Figs. 13, 19c). Its height varies from less than 1 m to several meters in old fans. The scarp is degraded and expressed as zone of steepened slope several tens of meters wide. Here, at the eastern end of the Almaty rangefront fault, we estimated ~3 m of vertical offset in a section which may represent a single-event scarp (Fig. 19c). We have no age control of the offset alluvial fans, but comparison with similar scarps elsewhere along the fault and in the vicinity indicate that it probably occurred after the LGM. The shape of the scarp also suggests that the last surface rupturing event did not occur in the very recent past.

4.3.3.3. Site S11

Site S11 is situated close to the *Selander et al.* [2012] study site (Figs. 13, 20). Here, a fault scarp that separates different generations of alluvial fans is expressed in the centre of the plateau between the high Zailisky Alatau and the Kazakh platform (Figs. 20, 21). The fans are incised by ephemeral channels as a result of recent uplift. We identified four different generations of fans T1 – T4 (youngest – oldest) based on their morphology, cross-cutting relationships, degree of dissection, and elevation (Fig. 21a). The fault scarp can be traced for approximately 10 km. All generations of fans are offset except the most recent river channels. The oldest fans show larger offsets than the younger ones (Fig. 21a, b).

We measured the height of the scarp at eight locations using DGPS profiles and the methods described above (Fig. 21a). Our profiles cover four different fan generations T1 - T4 and, therefore, return scarp heights that vary depending on the number of earthquakes that offset the alluvial fans since their abandonment (Fig. 21b).

The rather young and undissected fan surface T1 has an offset of only ~0.5 m (profile 7). This offset occurs south of the main scarp observed in neighbouring fans and may indicate a secondary fault strand.

Surface T2 is also rather smooth and affected by little incision. Our measurements show a vertical offset of ~2 m in profile 1 and of ~4 m in profile 8.

Fan surface T3 is more intensely dissected and higher than T1 and T2. It covers a smaller area because it has been partly eroded by later fan generations. Profiles 3-6 show that T3 is vertically offset by ~6-10 m and has very likely recorded multiple events.

Profile 2 reveals a cumulative, degraded scarp that offsets the oldest surface T4 by ~24 m. No sharp break in slope is visible here; instead, the scarp is a zone more than 150 m wide. We interpret this as the result of repeated offset in surface rupturing earthquakes and subsequent erosion and degradation of the scarp.

Without further dating we cannot distinguish whether T1 and T2 record a single earthquake only or multiple earthquakes. The larger offsets of 6-10 m in T3 likely indicate multiple events (Fig. 22). Terrace T4, with its 24 m high composite scarp, is interpreted to have formed in even more earthquakes.

5. Discussion

Our survey revealed a variety of geomorphic evidence for post-LGM/Holocene faulting along the Almaty section of the Zailisky-Alatau rangefront. We document thrust fault scarps at the rangefront and in alluvial fans (S1-S4, S6, S8-11), uplifted river terraces (S7), deformed soft sediments and folding in the foreland (W-NW of Almaty and the Kosmos site of *Macklin et al.*, [2015]), folding along the rangefront (S5), and backthrusts in the peneplain. We have shown that active deformation is not restricted to the immediate rangefront. Parallel fault strands are active in some places and deformation also extends into the foreland and the peneplain. Ongoing loess sedimentation over the past few millions years complicates the assessment of both short-term and long-term differential tectonic uplift as the aggrading loess changes the surface elevations and erosional properties. However, 50-100 m high scarps are

present along most of the rangefront. In the following we discuss the implications for the occurrence of large earthquakes, local fault segmentation, fault slip rates, seismic hazard, and the evolution of the Northern Tien Shan.

5.1. Earthquake magnitudes along the Almaty rangefront

The largest historical earthquake that occurred at or near the Almaty rangefront was the M~7.3 Verny Earthquake of 1887 [*Hay*, 1888; *Mushketov*, 1890; *Tatevossian*, 2007]. We did not find any fault offsets that appeared fresh enough in terms of scarp morphology and preservation to be likely related to this event only 130 years ago [cf. *Abdrakhmatov et al.*, 2016; *Arrowsmith et al.*, 2017; *Grützner et al.*, 2017 for examples of scarp preservation in the area]. Instead, at various sites along the rangefront, we observed degraded fault scarps in alluvial fans with heights of approximately 2-4 m. Palaeoseismological trenching could determine if these scarps represent single-event scarps or cumulative offsets. However, we note that for almost all sites we did not find any smaller scarps although different generations of alluvial surfaces were recognized. This observation may be explained by a climate-driven event of fan formation, probably related to the end of the LGM. In this case we would see single or multiple earthquake scarps in fans of similar age. Another explanation would be that the scarps do indeed represent single-event offsets, and that we do not observe smaller scarps because only the most recent event is preserved in the landscape, as is the case in the basin to the east of the Zailisky Alatau [*Grützner et al.*, 2017]. Given the rather long recurrence intervals of surface-breaking earthquakes in the Tien Shan [*Thompson*, 2001; *Campbell et al.*, 2015; *Abdrakhmatov et al.*, 2016; *Landgraf et al.*, 2016], the absence of smaller scarps and the state of degradation, we consider it likely that at least some of the 2-4 m high features were formed in single events in the Holocene. Larger amounts of vertical offsets are observed at various sites, but in all those cases, the presence of nearby smaller scarps suggests that these scarps formed in multiple events.

If these vertical offsets were related to single event scarps, they would likely correspond to paleo-earthquakes exceeding M6.8-7 [*Wells & Coppersmith*, 1994]. However, recent large reverse faulting events showed a remarkable variability of surface displacement. For example, no significant surface ruptures occurred in the 2015 Gorkha earthquake despite being a magnitude of M_W7.8 with an aftershock of M_W7.3 [*Wang & Fialko*, 2015; *Lindsey et al.*, 2015], with only centimetre-scale surface offsets observed on a subsidiary fault splay instead [*Elliott et al.*, 2016]. However, this earthquake ruptured a very gently-dipping fault plane of approximately 8° with a complex ramp and flat geometry. The 1992 Suusamyr earthquake struck in Kyrgyzstan (Western Tien Shan) with a magnitude of M_S7.3 on a much steeper dipping fault plane (~60°) [*Mellors et al.*, 1997]. It produced a rather unusual surface rupture pattern at two sites more than 25 km apart. One segment recorded up to 2.7 m of vertical offset with an extent of not more than 500 m. The second set of ruptures was more than 3 km long but showed much less than 2 m of vertical offset [*Bogachkin et al.*, 1997; *Ghose et al.*, 1997]. The two examples of Gorkha and Suusamyr and the observations from the 1887 Verny Earthquake illustrate that determining earthquake magnitudes from surface offsets may be of limited use in tectonic settings such as the Tien Shan. However, a 2-4 m high fault scarp certainly indicates a strong earthquake. Our estimate of M>6.8 for the scarps that we investigated must therefore be taken as a minimum value.

Instead of using surface offsets, information on magnitudes could be derived from the lengths of surface breaks. We found scarps of possible post-LGM age along the entire Almaty rangefront. Our observations cover a distance of more than 250 km along strike (Fig. 2). Empirical scaling relationships suggest a magnitude of ~8 for an earthquake with such a rupture length. Similar magnitudes and rupture lengths were reported for the 1889 Chilik earthquake [*Abdrakhmatov et al.*, 2016; *Krüger et al.*, 2015] and the 1911 Chon-Kemin event [*Delvaux et al.*, 2001; *Kulikova & Krüger*, 2015; *Arrowsmith et al.*, 2017]. However, the

surface offsets both in 1889 and 1911 were much greater than ~3 m. We found the distribution of possible single-event fault scarps along the rangefront to be scattered and, over large reaches, obscured by anthropogenic landscape modification. It is therefore not possible to identify potential sections marked by shorter, continuous scarps. This hampers any further speculation on surface rupture length vs. magnitude relations, and we have no evidence that the rangefront fault ruptured in its entire length in one event.

We also observe that the fault traces along the rangefront overlap and that individual fault strands and folds do not seem to exceed ~100 km in length. This may be interpreted as segmentation of the rangefront fault, which would mean that a rupture of the entire fault is somewhat less likely than smaller earthquake involving only parts of the rangefront. However, recent large earthquakes show that multiple faults can rupture in one event (e.g., Tabas, Iran [*Berberian,* 1979; *Walker et al.*, 2003] and Kaikoura, New Zealand [*Hamling et al.*, 2017]) and earthquakes may rupture multiple faults despite being separated by several kilometers [*Wesnousky,* 2006, 2008; *Abdrakhmatov et al.*, 2016; *Nissen et al.*, 2016]. We have no dating results that would support a single earthquake as the cause for all the possible single-event fault scarps that we observed. The pattern can also be explained with multiple smaller earthquakes along the Zailisky Alatau. This would imply that the rangefront does not necessarily release the accumulated stress along its entire length in a single large earthquake. Our study did not reveal systematic variations in the state of degradation of the fault scarps that would be evidence for multiple distinct ruptures. The lack of scarps along some sections of the rangefront could either be explained with blind faulting, inactivity since the LGM or in the Holocene, or partial erosion. Recent studies have, however, shown that faults in the Tien Shan tend to break in rare but exceptionally large events [*Deng et al.,* 1996; *Korjenkov et al.,* 2011; *Campbell et al.,* 2013, 2015; *Grützner et al.,* 2017]. We conclude that the Almaty

827 rangefront has been hit by surface rupturing earthquakes of M>6.8 and probably much
828 stronger in the recent past.

829

830 **5.2. Paleo-earthquake timing**

831 We do not have direct age measurements from the offset morphological markers except at site
832 S7, but our observations allow us to place constraints on the timing of the last surface
833 rupturing earthquakes. The 2-4 m high scarps offset alluvial fan surfaces that are only
834 minimally incised. Those fan surfaces probably correlate with a post-LGM terrace (10-15 ka)
835 observed in the Kyrgyz Tien Shan [*Korjenkov et al.*, 2002, 2007; *Thompson et al.*, 2002;
836 *Landgraf et al.*, 2016]. Rapid fan accumulation post-LGM is also reported from the Chinese
837 Tien Shan [e.g., *Avouac et al.*, 1993]. *Grützner et al.* [2017] found that fault scarps at the
838 nearby Toraigyr Fault were obliterated by erosion between 3.6 ka and ~17-40 ka. *Fitzsimmons*
839 *et al.* [2016] document the deposition of significant amounts of loess along the Zailisky
840 Alatau in the Holocene. These studies imply that it is unlikely for such a large number of
841 rather small fault scarps to have survived if they were pre-Holocene. We suggest that
842 probably all offsets of 2-3 m height that we document here are post-LGM and likely Holocene
843 in age. The occurrence of well-preserved multi-event scarps and the dating at site S7 further
844 indicate that not only one but several surface-rupturing earthquakes happened in the
845 Holocene.

846

847 **5.3. Seismic hazard and environmental effects**

848 The 1887 Verny Earthquake demonstrated that one type of threat for Almaty comes from
849 local faults that are right beneath or in the close vicinity of the city. Even if seismogenic
850 structures could not produce an earthquake exceeding M7.3, they pose a significant hazard in

851 terms of strong ground motion within the city limits. Earthquake environmental effects, like
852 landslides, and cascading effects like unstable landslide-dammed lakes, are an additional
853 concern in the rugged topography and thick loess deposits underlying the growing outskirts of
854 the city. Major landslides were documented in the steep loess hills in 1887 [*Mushketov*, 1890;
855 *Tatevossian*, 2007]. Those hills are now a major concern since they were subject to urban
856 development in the very recent past (Fig. 20). A surface-rupturing earthquake beneath
857 Almaty, such as the ones that we have detected as surface offsets in the alluvial fans, would
858 likely result in a large number of slope failures that affect now densely populated areas (Fig.
859 21a, b).

860 Our study shows that in contrast to what was learned from 1887, not only shaking but also
861 surface faulting must be taken into account. The effects of surface offset are somewhat
862 different from shaking in that such ruptures will cut utilities and crucial lifelines, block roads,
863 and damage critical infrastructure built on top. The Big Almaty Canal, for example, crosses
864 the rangefront fault several times and is, in significant parts, built directly on top of the
865 Holocene scarps. We point out that a future surface rupturing earthquake might severely
866 damage the canal with dire consequences for Almaty and for the settlements near the breach.

867 The two earthquakes that damaged Almaty in 1889 and 1911 happened far away from the
868 city, but due to their large magnitudes, caused devastating shaking in the city. A similar effect
869 can be expected from structures that we found to be active further away from Almaty. We
870 have shown that the entire area west and northwest of the city undergoes differential uplift,
871 recorded by the drainage pattern. This uplift might happen above blind faults in the Kazakh
872 platform whose lengths and offsets are entirely unknown. Post-LGM folding as far north as
873 Kosmos provides information on the scale of these structures. Also, in large parts of the
874 rangefront we observed more than one active fault strand. It is unknown whether or not they
875 can rupture together with other strands, or whether this happened in the past.

The fact that all the scarps that we found show strong degradation indicates that the last surface ruptures occurred a relatively long time, probably thousands of years, ago. If all the accumulated strain is released seismically and if the seismic cycle model can be applied to the Almaty rangefront [c.f. *Liu & Stein*, 2016], this may mean that the faults are loaded for thousands of years and that they are in a late stage of their cycle.

5.4. Evolution of the Zailisky Alatau

Our observations allow us to make some final remarks on the evolution of the Zailisky Alatau as a result of the far-field compressive stress caused by the collision of India and Eurasia. The uplifted Mesozoic peneplain (Fig. 2) not only is a well-preserved marker at intermediate elevations, but also controls the morphology of the highest parts of the range which are characterized by a remarkably flat top (Figs. 1b, 2a, 4c). This is probably evidence for relatively fast uplift, because otherwise the highest parts of the range would be more thoroughly eroded by the large rivers draining the Tien Shan. Our observations further indicate that at the onset of uplift in the Northern Tien Shan in the Upper Miocene, the active fault lay between the high Zailisky Alatau and the now uplifted peneplain (Fig. 23). The lack of Cenozoic sediments in the higher parts of the mountains may suggest that erosion was greatest in the most rapidly growing areas of the mountains and first stripped off most of the Paleogene and Neogene sedimentary cover. With sedimentary cover stripped, then the steep valleys in which rivers drain the mountain range today were carved into the underlying uplifted bedrock. However, it is not well resolved how thick the Cenozoic cover was and if it existed everywhere in the Northern Tien Shan.

The majority of our observations concern the Almaty rangefront fault. We show that this range is the most active structure of the Northern Tien Shan boundary today. The uplift of the peneplain to an intermediate elevation by this fault shows that fault activity then migrated

towards the Kazakh platform and a new fault formed or an inherited structure was re-activated. Consequently, another sector of the peneplain was uplifted. Further incision into the bedrock has created several steep canyons, but overall the old erosional surface is well preserved and a reliable marker of differential uplift.

Finally, we observe that the most recent generation of faults affects the Kazakh platform north of the mountain front. Evidence for this is found in soft-sediment deformation, local uplift, and folding. Again, we observe the basinward migration of fault activity. This uplift is at least partly related to blind faults that do not yet reach the surface. The backthrusts at the edge of the peneplain probably also formed relatively recently as they are prominent and not dissected. Backthrusts are usually associated with a change of fault dip at depth. In a ramp geometry, the fault steepens near the surface, leading to a space problem above that zone. Backthrusting is a way to accommodate the additional space by expelling a wedge of material (Fig. 23) [*Erickson*, 1995].

Despite the evidence for active tectonics in the Kazakh platform, the rangefront fault is still active, as recorded by the Holocene fault scarps. This is a feature that we observed all along the northern part of the Zailisky Alatau. Active deformation is not restricted to a single fault, but often distributed among a series of parallel structures. A similar observation was made for sets of normal faults in Greece [*Goldsworthy & Jackson*, 2001]: although fault activity migrates towards the basin, the other, more mature faults still show some level of activity. The propagation of active faulting towards the basins has been explained by applying the critical taper theory to accretionary wedges [*Davis et al., 1983*]. Similarly, *Dahlen et al.* [1984] used cohesive coulomb criteria to explain the mechanics of the propagation of the fold-and-thrust belt in western Taiwan. Our observations indicate that a similar mechanism may apply to the Northern Tien Shan. *Thompson et al.* [2002] show that the deformation is not concentrated along the frontal fault of the Kyrgyz Tien Shan, but occurs across a number

of distributed active structures. This is in agreement with geological observations from the Southern Tien Shan [*Thompson Jobe et al.*, 2017] and other mountain ranges [*Boyer*, 1992], analogue modelling [*Koyi et al.*, 2000], numerical experiments [*Willett*, 1999], GPS data from Central Asia [*Zubovich et al.*, 2010], and instrumental earthquakes throughout the Tien Shan [*Sloan et al.*, 2011].

The fate of the Kazakh platform north of Almaty is that of the peneplain: uplift will continue and erosion will strip off the Paleogene-Recent sediments on which Almaty is built, and a new peneplain bedrock surface will form. What is now the peneplain will become more intensely incised and further uplifted such that the clear morphological difference between the high Zailisky Alatau and the peneplain will decline.

6. Conclusions

We have shown that the Almaty rangefront has had surface-rupturing earthquakes in the Holocene and that active deformation can be found all along the northern front of the Zailisky Alatau. The record of tectonic shortening in the landscape encompasses fault scarps possibly from single and multiple events in alluvial fans, folding, uplifted abandoned river terraces, and backthrusts. We observe active structures not only at the main topographic step along the foothills, but also in the platform and in the mountains. The area west and north of Almaty experiences uplift and the city itself is located on the hanging wall of blind thrust fold deforming the foreland. We estimate that earthquakes of at least M>6.8-7 are necessary to produce the observed scarps if they resulted from single events. The 1887 Verny Earthquake did not rupture the surface as far as we know, which may imply that the surface ruptures that we found stem from stronger events (M>7.3). The state of scarp degradation implies that the causative earthquakes happened relatively long ago. This may have implications for seismic hazard, as the elapsed time since the last earthquake might be considered an indicator for

ongoing strain accumulation that brings the faults closer to failure. Quaternary dating of an uplifted river terrace east of Almaty allowed us to determine a Holocene uplift rate of 1-1.1 mm/a, which corresponds to a fault slip rate of about 1.2-2.2 mm/a depending upon the fault dip. This is the first slip rate measured along the rangefront, and represents not more than a quarter of the total shortening rate between Lake Issyk Kul and the Kazakh platform. Although the Zailisky Alatau has such impressive morphology, the slip rate is not extraordinarily high and is comparable to faults further west in Kyrgyzstan [*Thompson et al.*, 2002]. We show that the active faults pose a significant threat to Almaty since the city is built directly on top of the currently deforming structures. The fact that the geomorphic evidence for active faulting and folding has not been reported from the Almaty rangefront is partly due to the rather subtle geomorphological expression of active deformation, for example in Almaty and near Talgar. Other obstructions include the thick loess cover that blankets the foothills and partly obscures evidence of large ancient earthquakes, and the anthropogenic obliteration of fault scarps. High-resolution topographic data can, however, overcome these problems in many places. We emphasize the usefulness of employing high-resolution topography data such as stereo-satellite imagery, drone-based DEMs, and DGPS surveying.

Acknowledgements

This research was run under the Earthquakes without Frontiers project, funded by NERC and ESRC (Grant code: EwF_NE/J02001X/1_1), and within the Centre for Observation and Modelling of Earthquakes and Tectonics (COMET). SPOT imagery was acquired with a grant from EwF. The ALOS Global Digital Surface Model (AW3D30) is provided by and is copyright of JAXA. Corona and SRTM data are distributed by the Land Processes Distributed Active Archive Center (LP DAAC), located at USGS/EROS, Sioux Falls, SD, http://lpdaac.usgs.gov. The drone-DEMs will be made available through OpenTopography (www.opentopography.org). JRE is funded as a Royal Society University Research Fellow.

We thank Barry Parsons, Kathryn Fitzsimmons, and Tobi Sprafke for help and discussions in the field. Jessica Thompson Jobe, an anonymous reviewer, and the editor Taylor Schildgen provided valuable comments that helped to significantly improve the manuscript. Figure 1 was prepared with the Generic Mapping Tool software by *Wessel & Smith* [1998].

References

Abdrakhmatov, K.Y., Aldazhanov, S.A., Hager, B.H., Hamburger, M.W., Herring, T.A., Kalabaev, K.B., Makarov, V.I., Molnar, P., Panasyuk, S.V., Prilepin, M.T., Reilinger, R.E., Sadybakasovstar, I.S., Souter, B.J., Trapeznikov, Yu.A., Tsurkov, V.Ye., & Zubovich, A.V., 1996. Relatively recent construction of the Tien Shan inferred from GPS measurements of present-day crustal deformation rates. Nature 384, 450–453. http://dx.doi.org/10.1038/384450a0.

Abdrakhmatov, K., Weldon, R. J., Thompson, S. C., Burbank, D. W., Rubin, C., Miller, M., & Molnar, P., 2001. Onset, style and current rate of shortening in the central Tien Shan, Kyrgyz Republic. Russian Geology and Geophysics, 42(10), 1585-1609.

Abdrakhmatov, K. Y., Djanuzakov, K. D., & Delvaux, D., 2002. Active tectonics and seismic hazard of the Issyk-Kul basin in the Kyrgyz Tian-Shan. Lake Issyk-Kul: Its Natural Environment, 13, 147-160.

Abdrakhmatov, K., Walker, R.T., Campbell, G.E., Carr, A.S., Elliott, A., Hillemann, C., Hollingsworth, J., Landgraf, A., Mackenzie, D., Mukambayev, A., Rizza, M., & Sloan, R.A., 2016. Multi-segment rupture in the July 11th 1889 Chilik earthquake (Mw 8.0–8.3), Kazakh Tien Shan, identified from remote-sensing, field survey, and palaeoseismic trenching. J. Geophys. Res., Solid Earth121 (6), 4615–4640. http://dx.doi.org/10.1002/2015JB012763.

997 Arrowsmith, J. R., Crosby, C. J., Korzhenkov, A. M., Mamyrov, E., Povolotskaya, I.,
998 Guralnik, B., & Landgraf, A., 2017. Surface rupture of the 1911 Kebin (Chon–Kemin)
999 earthquake, Northern Tien Shan, Kyrgyzstan. Geological Society, London, Special
1000 Publications, 432(1), 233-253.

1001 Atrushkevitch, P. A., Kalabaev, N. B., Kartashov, A. P., Lototsky, V. D., & Ostropico, P. A.,
1002 1988. Research on crustal movements on the Alma-Ata polygon, Northern Tien Shan. Journal
1003 of Geodynamics, 9(2-4), 279-292.

1004 Avouac, J.P., Tapponnier, P., Bai, M., You, H., & Wang, G., 1993. Active thrusting and
1005 folding along the northern Tien Shan and late Cenozoic rotation of the Tarim relative to
1006 Dzungaria and Kazakhstan. J. Geophys. Res., Solid Earth 98 (B4), 6755–6804.
1007 http://dx.doi.org/10.1029/92JB01963.

1008 Bemis, S. P., Micklethwaite, S., Turner, D., James, M. R., Akciz, S., Thiele, S. T., &
1009 Bangash, H. A., 2014. Ground-based and UAV-based photogrammetry: A multi-scale, high-
1010 resolution mapping tool for structural geology and paleoseismology. Journal of Structural
1011 Geology, 69, 163-178.

1012 Berberian, M., 1979. Earthquake faulting and bedding thrust associated with the Tabas-e-
1013 Golshan (Iran) earthquake of September 16, 1978. Bulletin of the Seismological Society of
1014 America, 69(6), 1861-1887.

1015 Bindi, D., Parolai, S., Gómez-Capera, A., Locati, M., Kalmetyeva, Z., & Mikhailova, N.,
1016 2014. Locations and magnitudes of earthquakes in Central Asia from seismic intensity data. J.
1017 Seismol.18 (1), 1–21. http://dx.doi.org/10.1007/s10950-013-9392-1.

1018 Bogachkin, B. M., Korzhenkov, A. M., Mamyrov, E., Nechaev, Y. V., Omuraliev, M.,
1019 Petrosyan, A. E., Pletnev, K. G., Rogozhin, E. A., & Charimov, T. A., 1997. The structure of

the 1992 Susamyr earthquake source based on its geological and seismological manifestations. Izvestiya Physics of the Solid Earth, 33(11), 867-882.

Bogdanovich, K.I., Kark, I.M., Korolkov, B.Y., & Mushketov, D.I., 1914. Earthquake in Northern District of Tien Shan, 22 December 1910 (4 January 1911). Commission of the Geology Committee, Leningrad (in Russian).

Bowman, D., Korjenkov, A., Porat, N., & Czassny, B., 2004. Morphological response to Quaternary deformation at an intermontane basin piedmont, the northern Tien Shan, Kyrghyzstan. Geomorphology, 63(1), 1-24.

Boyer, S. E., 1992. Geometric evidence for synchronous thrusting in the southern Alberta and northwest Montana thrust belts. In: McClay, K. R. (ed.), Thrust Tectonics, Chapman and Hall, New York, 377– 390.

Brown, E.T., Bourlés, D.L., Burchfiel, B.C., Qidong, D., Jun, L., Molnar, P., Raisbeck, G.M., & Yiou, F., 1998. Estimation of slip rates in the southern Tien Shan using cos-mic ray exposure dates of abandoned alluvial fans. Geol. Soc. Am. Bull.110 (3), 377–386. http://dx.doi.org/10.1130/0016-7606(1998)110<0377:EOSRIT>2.3.CO;2.

Bull, W., & McFadden L., 1977. Tectonic geomorphology north and south of the Garlock fault, California. In: Doehring, D. E. (ed.), Geomorphology in Arid Regions, Proceedings 8th Annual Geomorphology Symposium, State University of New York, Binghampton, 115-137.

Bullen, M. E., Burbank, D. W., & Garver, J. I., 2003. Building the northern Tien Shan: Integrated thermal, structural, and topographic constraints. The Journal of Geology, 111(2), 149-165.

1041 Burbank, D. W., McLean, J. K., Bullen, M., Abdrakhmatov, K. Y., & Miller, M. M., 1999.
1042 Partitioning of intermontane basins by thrust-related folding, Tien Shan, Kyrgyzstan. Basin
1043 Research, 11(1), 75-92.

1044 Burgette, R. J., Weldon, R. J., Abdrakhmatov, K. Y., Ormukov, C., Owen, L. A., &
1045 Thompson, S. C., 2017. Timing and process of river and lake terrace formation in the Kyrgyz
1046 Tien Shan. Quaternary Science Reviews, 159, 15-34.

1047 Burtman, V. S., 1975. Structural geology of Variscan Tien Shan, USSR. American Journal of
1048 Science, 275-a, 157-186.

1049 Buslov, M. M., Kokh, D. A., & De Grave, J., 2008. Mesozoic-Cenozoic tectonics and
1050 geodynamics of Altai, Tien Shan, and Northern Kazakhstan, from apatite fission-track data.
1051 Russian Geology and Geophysics, 49(9), 648-654.

1052 Campbell, G. E., Walker, R. T., Abdrakhmatov, K., Schwenninger, J. L., Jackson, J. A.,
1053 Elliott, J. R., & Copley, A. C., 2013. The Dzhungarian fault: Late Quaternary tectonics and
1054 slip rate of a major right-lateral strike-slip fault in the northern Tien Shan region. Journal
1055 Geophysical Research, 118, 5681-5698, doi:10.1002/jgrb.50367.

1056 Campbell, G. E., Walker, R. T., Abdrakhmatov, K., Jackson, J. A., Elliott, J. R., Mackenzie,
1057 D., Middleton, T., & Schwenninger, J. L., 2015. Great earthquakes in low strain rate
1058 continental interiors: An example from SE Kazakhstan. Journal Geophysical Research, 120,
1059 5507-5534, doi:10.1002/2015JB011925.

1060 Clark, P. U., Dyke, A. S., Shakun, J. D., Carlson, A. E., Clark, J., Wohlfarth, B., Mitrovica, J.
1061 X., Hostetler, S.W., & McCabe, A. M., 2009. The last glacial maximum. Science, 325(5941),
1062 710-714.

1063 CMT, 2016. Global Centroid–Moment–Tensor (CMT) catalog. CMT catalog web search,
1064 http://www.globalcmt.org/CMTsearch.html. Last access 25 December 2016.

1065 Crosby, C. J., Arrowsmith, J. R., Korjenkov, A. M., Guralnik, B., Mamyrov, E., &
1066 Povolotskaya, I. E., 2007. The hunt for surface rupture from the 1889 Ms 8.3 Chilik
1067 earthquake, northern Tien Shan, Kyrgyzstan and Kazakhstan. In: AGU Fall Meeting
1068 Abstracts, Dec 2007.

1069 Cuenca, M. C., Hooper, A. J., & Hanssen, R. F., 2013. Surface deformation induced by water
1070 influx in the abandoned coal mines in Limburg, The Netherlands observed by satellite radar
1071 interferometry. Journal of Applied Geophysics, 88, 1-11.

1072 Dahlen, F. A., Suppe, J., & Davis, D., 1984. Mechanics of fold-and-thrust belts and
1073 accretionary wedges: Cohesive Coulomb theory. Journal of Geophysical Research: Solid
1074 Earth, 89(B12), 10087-10101.

1075 Davis, D., Suppe, J., & Dahlen, F. A. 1983. Mechanics of fold-and-thrust belts and
1076 accretionary wedges. Journal of Geophysical Research: Solid Earth, 88, 1153–1172.

1077 Delvaux, D., Abdrakhmatov, K. E., Lemzin, I. N., & Strom, A. L., 2001. Landslide and
1078 surface breaks of the 1911 M 8.2 Kemin Earthquake. Landslides, 42(10), 1583-1592.

1079 Deng, Q., Zhang, P., Xu, X., Yang, X., Peng, S., & Feng, X., 1996. Paleoseismology of the
1080 northern piedmont of Tianshan Mountains, northwestern China. Journal of Geophysical
1081 Research: Solid Earth, 101(B3), 5895-5920.

1082 Elliott, J. R., R. Jolivet, P. Gonzalez, J.-P. Avouac, J. Hollingsworth, M. Searle & V. Stevens,
1083 2016. Himalayan Megathrust Geometry and Relation to Topography Revealed by the Gorkha
1084 Earthquake. Nature Geoscience, 9, 174-180, doi:10.1038/NGEO2623.

1085 Engdahl, E., Van Der Hilst, R., Buland, R., 1998. Global teleseismic earthquake reloca-tion
1086 with improved travel times and procedures for depth determination. Bull. Seismol. Soc.
1087 Am.88 (3), 722–743.

1088 England, P., & Molnar, P., 2015. Rheology of the lithosphere beneath the central and western
1089 Tien Shan. Journal of Geophysical Research: Solid Earth, 120(5), 3803-3823.

1090 Erickson, S. G., 1995. Mechanics of triangle zones and passive-roof duplexes: implications of
1091 finite-element models. Tectonophysics, 245(1), 1-11.

1092 Fitzsimmons, K. E., Sprafke, T., Zielhofer, C., Günter, C., Deom, J. M., Sala, R., & Iovita, R.,
1093 2016. Loess accumulation in the Tian Shan piedmont: Implications for palaeoenvironmental
1094 change in arid Central Asia. Quaternary International,
1095 http://dx.doi.org/10.1016/j.quaint.2016.07.041.

1096 Ghose, S., Mellors, R. J., Korjenkov, A. M., Hamburger, M. W., Pavlis, T. L., Pavlis, G. L.,
1097 Omuraliev, M., Mamyrov, E., & Muraliev, A. R., 1997. The M_S= 7.3 1992 Suusamyr,
1098 Kyrgyzstan, earthquake in the Tien Shan: 2. Aftershock focal mechanisms and surface
1099 deformation. Bulletin of the Seismological Society of America, 87(1), 23-38.

1100 Goldsworthy, M., & Jackson, J., 2001. Migration of activity within normal fault systems:
1101 examples from the Quaternary of mainland Greece. Journal of Structural Geology, 23(2), 489-
1102 506.

1103 Gorshkov, G. P., 1947. Tectonic earthquakes and seismic zonation of the territory of the
1104 USSR. Foundation IFS AN USSR (in Russian).

1105 Goryachev, A. V., 1959. Mesozoic-Cenozoic Structure, History, Tectonic Development, and
1106 Seismicity of the Regions of the Lake Issyk-Kul. Academy of Sciences Publishing House,
1107 Moscow (in Russian).

1108 Grützner, C., Carson, E., Walker, R. T., Rhodes, E. J., Mukambayev, A., Mackenzie, D.,
1109 Elliott, J. R., Campbell, G., & Abdrakhmatov, K., 2017. Assessing the activity of faults in
1110 continental interiors: Palaeoseismic insights from SE Kazakhstan. Earth and Planetary
1111 Science Letters, 459, 93-104.

1112 Hall, M. E., 1997. Towards an absolute chronology for the Iron Age of Inner Asia. Antiquity,
1113 71(274), 863-874.

1114 Hamling, I. J., Hreinsdóttir, S., Clark, K., Elliott, J., Liang, C., Fielding, E., Litchfield, N.,
1115 Villamor, P., Wallace, L., Wright, T. J., D'Anastasio, E., Bannister, S., Burbidge, D., Denys,
1116 P., Gentle, P., Howarth, J., Mueller, C., Palmer, N., Pearson, C., Power, W., Barnes, P.,
1117 Barrell, D. J. A., Van Dissen, R., Langridge, R., Little, T., Nico, A., Pettinga, J., Rowland, J.,
1118 & Stirling, M., 2017. Complex multifault rupture during the 2016 Mw 7.8 Kaikōura
1119 earthquake, New Zealand. Science, eaam7194.

1120 Hay, M. B., 1888. The earthquakes of May and June, 1887, in the Verny (Vernoe) District,
1121 Russian Turkestan, and their consequences. Proceedings of the Royal Geographical Society
1122 and Monthly Record of Geography, 10(10) 638-646.

1123 ISC, 2016. International Seismological Centre, on-line catalog. http://www.isc.ac.uk.
1124 International Seismological Centre, Thatcham, UK. Last access 12 December 2016.

1125 Kondorskaya, N., & Shebalin, N., 1977. New Catalog of Strong Earthquakes in the Territory
1126 of the USSR from Ancient Times to 1975, Academy of Sciences, Moscow (English
1127 translation, updated through 1977, available as Report SE-31, World Data Center A for Solid
1128 Earth Geophysics, Boulder, CO, 606 pp.

1129 Koppes, M., Gillespie, A. R., Burke, R. M., Thompson, S. C., & Stone, J., 2008. Late
1130 Quaternary glaciation in the Kyrgyz Tien Shan. Quaternary Science Reviews, 27(7), 846-866.

Korjenkov, A. M., Kovalenko, V. A., & Usmanov, S. F., 2002. Long-term preservation of Paleoseismic deformation as a tool for revealing traces of ancient seismic catastrophes (example of the Chon-Kemin Valley, Kyrgyzstan). Kartographische Bausteine, 28, 137-154.

Korjenkov, A. M., Arrowsmith, J. R., Crosby, C., Mamyrov, E., Orlova, L. A., Povolotskaya, I. E., & Tabaldiev, K., 2006. Seismogenic destruction of the Kamenka medieval fortress, northern Issyk-Kul region, Tien Shan (Kyrgyzstan). Journal of Seismology, 10(4), 431-442.

Korjenkov, A. M., Povolotskaya, I. E., & Mamyrov, E., 2007. Morphologic expression of Quaternary deformation in the northwestern foothills of the Ysyk-Köl basin, Tien Shan. Geotectonics, 41(2), 130-148.

Korjenkov, A. M., Abdieva, S. V., Vakhrameeva, P. S., Dzhumabaeva, A. B., Mamyrov, E., Morozova, E. A., Orlova, L. A. &, Fortuna, A. B., 2011. Strong historical earthquakes in the northwestern Issyk Kul'basin (northern Tien Shan). Russian Geology and Geophysics, 52(9), 955-962.

Koyi, H. A., Hessami, K., & Teixell, A., 2000. Epicenter distribution and magnitude of earthquakes in fold-thrust belts: insights from sandbox models. Geophys. Res. Lett., 27, 273–276.

Krüger, F., Kulikova, G., & Landgraf, A., 2015. Instrumental magnitude constraints for the 11 July 1889, Chilik earthquake. Geological Society, London, Special Publications, 432(1), 41-72.

Kulikova, G., & Krüger, F., 2015. Source process of the 1911 M8. 0 Chon-Kemin earthquake: investigation results by analogue seismic records. Geophysical Journal International, 201(3), 1891-1911.

1153 Landgraf, A., Dzhumabaeva, A., Abdrakhmatov, K. E., Strecker, M. R., Macaulay, E. A.,
1154 Arrowsmith, J. R., Sudhaus, H., Preusser, F., Rugel, G., & Merchel, S., 2016. Repeated large-
1155 magnitude earthquakes in a tectonically active, low-strain continental interior: The northern
1156 Tien Shan, Kyrgyzstan. Journal of Geophysical Research: Solid Earth, 121(5), 3888-3910.

1157 Lindsey, E. O., Natsuaki, R., Xu, X., Shimada, M., Hashimoto, M., Melgar, D., & Sandwell,
1158 D. T., 2015. Line-of-sight displacement from ALOS-2 interferometry: Mw 7.8 Gorkha
1159 earthquake and Mw 7.3 aftershock. Geophysical Research Letters, 42(16), 6655-6661.

1160 Liu, M., & Stein, S., 2016. Mid-continental earthquakes: Spatiotemporal occurrences, causes,
1161 and hazards. Earth-Science Reviews, 162, 364-386.

1162 Machalett, B., Frechen, M., Hambach, U., Oches, E.A., Zöller, L., & Markovic, S.B., 2006.
1163 The loess sequence from Remisowka (northern boundary of the Tien Shan Mountains,
1164 Kazakhstan) - Part I: luminescence dating. Quaternary International, 152-153, 192-201.

1165 Mackenzie, D., Elliott, J. R., Altunel, E., Walker, R. T., Kurban, Y. C., Schwenninger, J. L.,
1166 & Parsons, B., 2016. Seismotectonics and rupture process of the Mw 7.1 2011 Van reverse
1167 faulting earthquake, Eastern Turkey, and implications for hazard in regions of distributed
1168 shortening. Geophysical Journal International, 206, 501-524, doi:10.1093/gji/ggw158.

1169 Mackenzie, D., & Elliott, A. J., 2017. Untangling tectonic slip from the potentially misleading
1170 effects of landform geometry. Geosphere, 13(4), doi:10.1130/GES01386.1.

1171 Macklin, M. G., Panyushkina, I. P., Toonen, W. H., Chang, C., Tourtellotte, P. A., Duller, G.
1172 A., Wang, H., & Prins, M. A., 2015. The influence of Late Pleistocene geomorphological
1173 inheritance and Holocene hydromorphic regimes on floodwater farming in the Talgar
1174 catchment, southeast Kazakhstan, Central Asia. Quaternary Science Reviews, 129, 85-95.

1175 Makarov, V. I., 1977. New tectonic structures of the Central Tien Shan. Moscow, Order of the
1176 Red Banner Geology Institute, Akad. Sci., 171 p. (in Russian).

1177 Mellors, R. J., Vernon, F. L., Pavlis, G. L., Abers, G. A. , Hamburger, M. W., Ghose, S., &
1178 Iliasov, B., 1997. The Ms = 7.3 1992 Suusamyr, Kyrgyzstan, Earthquake: Constraints on
1179 Fault Geometry and Source Parameters Based on Aftershocks and Body-Wave Modeling.
1180 Bulletin of the Seismological Society of America, 87(1), 11-22.

1181 Mikhailova, N. N., Sokolova, I. N., Velikanov, A. Y., & Sokolov, A. N., 2015. Earthquakes
1182 on the territory of Almaty, Vestnyk NYAC RK, 3, 87-93.

1183 Mushketov, I. V., 1890. Le tremblement de terre de Verny, 28 Mai (9 Juin) 1887. Memoires
1184 du Comite Geologique, X(1).

1185 Mushketov, I. V., & Orlov, A. P., 1893. Catalogue of earthquakes in the Russian Empire, Zap.
1186 RGO, 26 (in Russian).

1187 Nalivkin, D. V., 1983. Geological map of the USSR and adjoining water-covered areas.
1188 Leningrad, Ministry of Geology of the USSR, Karpinsky All-Union Order of Lenin
1189 Geological Research Institute, scale 1:2,500,000.

1190 Nissen, E., Elliott, J. R., Sloan, R. A., Craig, T. J., Funning, G. J., Hutko, A., Parsons, B. E.,
1191 & Wright, T. J., 2016. Limitations of rupture forecasting exposed by instantaneously triggered
1192 earthquake doublet. Nature Geoscience 9, 330–336.

1193 Oskin, M. E., & Burbank, D., 2007. Transient landscape evolution of basement-cored uplifts:
1194 Example of the Kyrgyz Range, Tian Shan. Journal of Geophysical Research: Earth Surface,
1195 112(F3).

1196 QGIS Development Team, 2017. QGIS Geographic Information System. Open Source
1197 Geospatial Foundation Project. http://www.qgis.org/

1198 Reimer, P.J., Bard, E., Bayliss, A., Beck, J.W., Blackwell, P.G., Bronk Ramsey, C., Buck,
1199 C.E., Cheng, H., Edwards, R.L., Friedrich, M., Grootes, P.M., Guilderson, T.P., Hafl-idason,
1200 H., Hajdas, I., Hatté, C., Heaton, T.J., Hoffmann, D.L., Hogg, A.G., Hughen, K.A., Kaiser,
1201 K.F., Kromer, B., Manning, S.W., Niu, M., Reimer, R.W., Richards, D.A., Scott, E.M.,
1202 Southon, J.R., Staff, R.A., Turney, C.S.M., & van der Plicht, J., 2013. Int-Cal13 and
1203 Marine13 radiocarbon age calibration curves 0–50,000 years cal BP. Radiocarbon55 (4),
1204 1869–1887. http://dx.doi.org/10.1017/S0033822200048864.

1205 Riley, S. J., DeGloria, S. D., & Elliot, R., 1999. A terrain ruggedness index that quantifies
1206 topographic heterogeneity. Intermountain Journal of Sciences, 5, 23-27.

1207 Sala, R., & Deom, J.M., 2005. Petroglyphs of South Kazakhstan. Laboratory of
1208 Geoarchaeology, Almaty, Kazakhstan, 150 p., ISBN 9965-27-645-5.

1209 Selander, J., Oskin, M., Ormukov, C., & Abdrakhmatov, K., 2012. Inherited strike-slip faults
1210 as an origin for basement-cored uplifts: Example of the Kungey and Zailiskey ranges,
1211 northern Tian Shan. Tectonics, 31(4).

1212 Sloan, R.A., Jackson, J.A., McKenzie, D., & Priestley, K., 2011. Earthquake depth distri-
1213 butions in central Asia, and their relations with lithosphere thickness, short-ening and
1214 extension. Geophys. J. Int.185 (1), 1–29. http://dx.doi.org/10.1111/j.1365-
1215 246X.2010.04882.x.

1216 Smekalin, O. P., Imaev, V. S., Korzhenkov, A. M., & Chipizubov, A. V., 2016.
1217 Paleoseismological investigations in the pleistoseismal zone of the 1885 Belovodskoe
1218 earthquake, North Tien Shan. Seismic Instruments, 52(4), 279-289.

1219 Smith, B., & Sandwell, D., 2003. Accuracy and resolution of shuttle radar topography mission
1220 data. Geophysical Research Letters, 30(9), 1467, doi:10.1029/2002GL016643.

1221 Sobel, E. R., Oskin, M. E., Burbank, D. W., & Mikolaichuk A., 2006. Exhumation of
1222 basement-cored uplifts: Example of the Kyrgyz Range quantified with apatite fission-track
1223 thermochronology. Tectonics, 25, TC2008, doi:10.1029/2005TC001809.

1224 Takeuchi, N., Fujita, K., Aizen, V. B., Narama, C., Yokoyama, Y., Okamoto, S., Naoki, K., &
1225 Kubota, J., 2014. The disappearance of glaciers in the Tien Shan Mountains in Central Asia at
1226 the end of Pleistocene. Quaternary Science Reviews, 103, 26-33.

1227 Tatevossian, R. E. , 2007. The Verny, 1887, earthquake in Central Asia: Application of the
1228 INQUA scale, based on coseismic environmental effects. Quaternary International, 173, 23-
1229 29.

1230 Thompson, S. C., 2001. Active tectonics in the central Tien Shan, Kyrgyz Republic, PhD
1231 thesis, Univ. of Washington, Wash.

1232 Thompson, S.C., Weldon, R.J., Rubin, C.M., Abdrakhmatov, K., Molnar, P., & Berger, G.W.,
1233 2002. Late Quaternary slip rates across the central Tien Shan, Kyrgyzstan, central Asia. J.
1234 Geophys. Res., Solid Earth107 (B9), ETG-7. http://dx.doi.org/10.1029/2001JB000596.

1235 Thompson Jobe, J. A., Li, T., Chen, J., Burbank, D. W., & Bufe, A., 2017. Quaternary
1236 Tectonic Evolution of the Pamir-Tian Shan Convergence Zone, Northwest China. Tectonics,
1237 doi:10.1002/2017TC004541.

1238 Tibaldi, A., Graziotto, E., Forcella, F., & Gapich, V. H., 1997. Morphotectonic indicators of
1239 Holocene faulting in central Tien Shan, Kazakstan, and geodynamic implications. Journal of
1240 Geodynamics, 23(1), 23-45.

1241 Torizin, J., Jentzsch, G., Malischewsky, P., Kley, J., Abakanov, T., & Kurskeev, A., 2009.
1242 Rating of seismicity and reconstruction of the fault geometries in northern Tien Shan within

1243 the project “Seismic Hazard Assessment for Almaty”. Journal of Geodynamics, 48(3), 269-
1244 278.

1245 Walker, R., Jackson, J., & Baker, C., 2003. Surface expression of thrust faulting in eastern
1246 Iran: source parameters and surface deformation of the 1978 Tabas and 1968 Ferdows
1247 earthquake sequences. Geophysical Journal International, 152(3), 749-765.

1248 Wang, K. & Fialko, Y., 2015. Slip model of the 2015 Mw 7.8 Gorkha (Nepal) earthquake
1249 from inversions of ALOS-2 and GPS data. Geophys. Res. Lett. 42, 7452–7458.

1250 Wells, D. L., & Coppersmith, K. J., 1994. New empirical relationships among magnitude,
1251 rupture length, rupture width, rupture area, and surface displacement. Bulletin of the
1252 Seismological Society of America, 84(4), 974-1002.

1253 Wesnousky, S. G., 2006. Predicting the endpoints of earthquake ruptures. Nature 444, 358–
1254 360.

1255 Wesnousky, S. G., 2008. Displacement and geometrical characteristics of earthquake surface
1256 ruptures: issues and implications for seismic-hazard analysis and the process of earthquake
1257 rupture. Bull. Seismol. Soc. Am. 98, 1609–1632.

1258 Wessel, P., & Smith, W.H., 1998. New improved version of generic mapping tools released.
1259 Eos Trans. AGU79 (47), 579. http://dx.doi.org/10.1029/98EO00426.

1260 Willett, S. D., 1999. Rheological dependence of extension in wedge models of convergent
1261 orogens. Tectonophysics, 305(4), 419-435.

1262 Windley, B. F., Allen, M. B., Zhang, C., Zhao, Z. Y., & Wang, G. R., 1990. Paleozoic
1263 accretion and Cenozoic redeformation of the Chinese Tien Shan range, central Asia. Geology,
1264 18(2), 128-131.

1265 Zech, R., 2012. A late Pleistocene glacial chronology from the Kitschi-Kurumdu Valley, Tien
1266 Shan (Kyrgyzstan), based on ^{10}Be surface exposure dating. Quaternary Research, 77(2), 281-
1267 288.

1268 Zubovich, A.V., Wang, X., Scherba, Y.G., Schelochkov, G.G., Reilinger, R., Reigber, C.,
1269 Mosienko, O.I., Molnar, P., Michajljow, W., Makarov, V.I., Li, J., Kuzikov, S.I., Herring,
1270 T.A., Hamburger, M.W., Hager, B.H., Dang, Y., Bragin, V.D., Beisenbaev, R.T., 2010. GPS
1271 velocity field for the Tien Shan and surrounding regions. Tectonics29.
1272 http://dx.doi.org/10.1029/2010TC002772.

1273

Tables

Table 1

Site	Coordinates	Type of deformation	Offset	Age	Slip rate	Comment	Figures
S1 Akterek	N43.211° E75.573°	Offset alluvial fans	2.2-2.5 m	unknown, probably ~LGM or Holocene, pre-dates kurgans	-	elevation profiles from drone-DEM	5, 6
S2 Akterek	N43.227° E75.612°	Offset alluvial fans and river terraces	6-7 m	unknown, probably pre-LGM, pre-dates kurgans	-	elevation profiles from drone-DEM	5, 6
S3 Fabrichny	N43.152° E76.446°	Offset alluvial fan	1 m	unknown, probably ~LGM or Holocene, pre-dates kurgans	-	-	7
S4 Almaty	N43.239° E76.948°	Offset alluvial fan	5-7 m	unknown	-	elevation profiles from SPOT6-DEM	9
S5 Talgar	N43.296° E77.214°	Offset alluvial fan and folding (blind thrust)	5 m	unknown	-	elevation profiles from SRTM1 and JAXA DEMs	10
S6 Rahat	N43.368° E77.371°	Offset river terraces	5-11 m	unknown, youngest terraces probably Holocene	-	elevation profiles from drone-DEM	11, 12
S7 Slip rate site near Chilik	N43.491° E78.136°	Offset river terraces	9-50 m	terrace with 14 m offset is 13.3-15 ka	1.2-2.2 mm/a in the Holocene	elevation profiles from drone-DEM	14-17
S8 Big Almaty Canal	N43.488° E78.155°	Offset alluvial fans	unknown	unknown, probably ~LGM	-	-	18
S9 Gravels east of Chilik	N43.498° E78.270°	Deformed gravels - fault-propagation fold?	-	unknown	-	-	19b
S10 Alluvial fan east of Chilik	N43.505° E78.490°	Offset alluvial fans	1-3 m, several higher scarps also visible	unknown, probably ~LGM or Holocene, pre-dates kurgans	-	-	19c
S11 *Selander et al.* [2012] study site	N43.432° E78.298°	Offset alluvial fans	0.5-24 m	youngest surfaces probably ~LGM or Holocene, older terraces estimated to be 100±30 ka based on data from Q2 terraces in other parts of the Tien Shan [*Selander et al., 2012*]	0.8±0.5 mm/a and 0.43±0.3 mm/a [*Selander et al., 2012*]	elevation profiles from DGPS data	21, 22
Western Zailisky Alatau, Peneplain south of Ushkonyr	N43.089° E76.499°	Fault scarps in peneplain surface	unknown	unknown	-	-	2

Uplift NW of Almaty	N43.310° E76.811°	Uplift of the foreland sediments and stream incision, blind thrusts or folding	unknown	unknown	-	-	8
Kosmos	N43.531° E77.281°	Folded and offset glaciofluvial deposits	small-scale folding	17.1±0.22 ka BC	-	site described and dated by *Macklin et al.* [2015]	8

Table 2

Sample	**Lab code**	**Material and pretreatment**	**d13C**	**Conventional age**	**2 sigma calibration**	**D14C**
chilik-2016-upper	Beta443448	(organic sediment): acid washes	-21.7	12,770 ± 70 BP	Cal BC 13,410 to 13,125 (Cal BP 15,360 to 15,075)	-796.0 ± 1.8 ‰
chilik-2016-middle	Beta443449	(charred material): acid/alkali/acid	-23.7	11,470 ± 50 BP	Cal BC 11,475 to 11,265 (Cal BP 13,425 to 13,215)	-760.2 ± 1.5 ‰
chilik-2016-lower	Beta443450	(charred material): acid/alkali/acid	-25.5	11,580 ± 150 BP	Cal BC 11,785 to 11,165 (Cal BP 13,735 to 13,115)	-763.4 ± 4.4 ‰

Table captions

Table1: Overview of the study sites discussed in this paper.

Table 2: Results from 14C dating of the three samples at site S7. Dating was performed by BETA Analytic (Miami, FL, USA). INTCAL13 was used for calibration [Reimer et al., 2013].

Figures

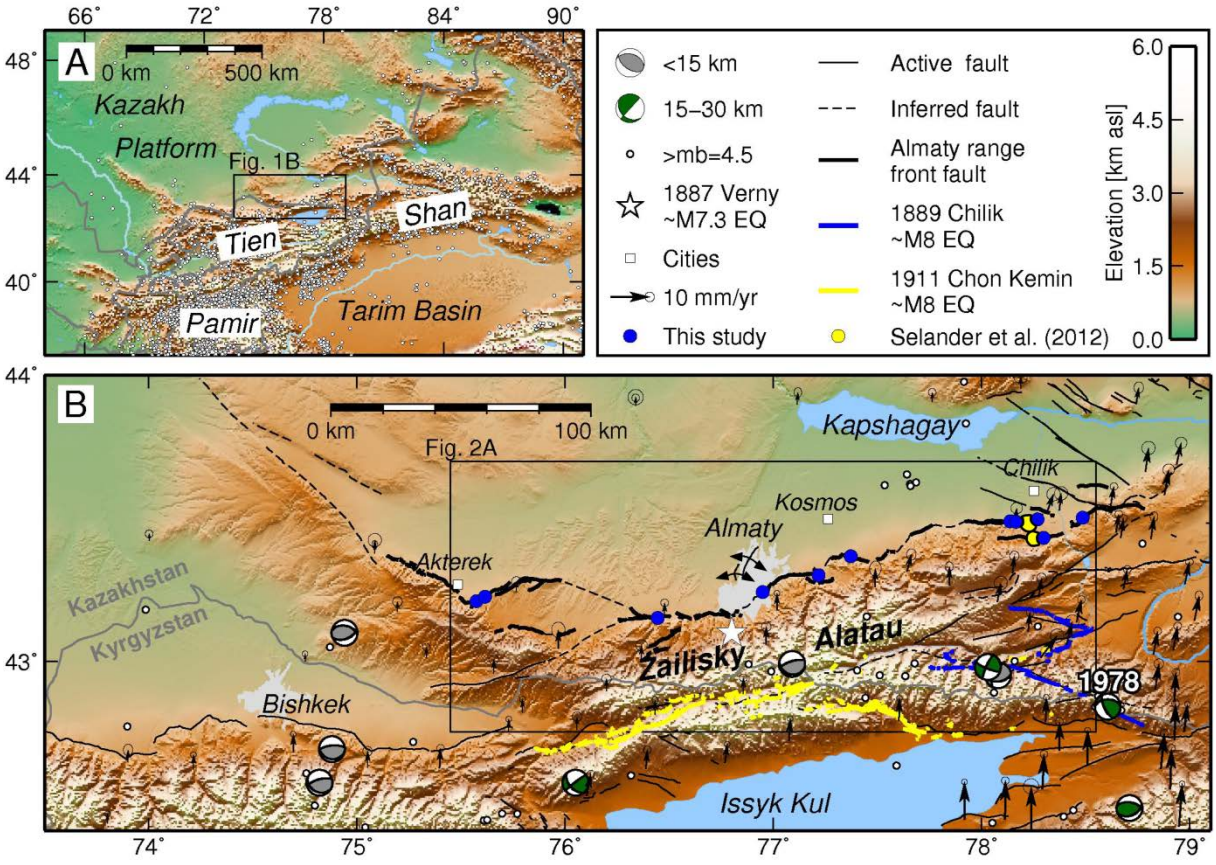

Figure 1. Tectonic setting in Central Asia of our study area of the Zailisky Alatau within the Tien Shan. (a) Instrumental seismicity is focussed within the Pamir and around the margins of the Tarim Basin. (b) The Almaty rangefront fault marks the northern boundary of the Zailisky Alatau (black line). Blue dots denote the sites discussed in detail in this paper, yellow dots show the location of the slip rate estimate of Selander et al. [2012]. Beachballs show depth-coloured earthquakes with focal mechanisms from body-waveform modelling of Sloan et al. [2011]. The location of the 1978 Dzhalanash–Tyup earthquake is marked (location from Krüger et al. [2015] and focal data from CMT [2016]).White dots are earthquakes mb>4.5 from the catalog of Engdahl et al. [1998] from 1960–2008 and the ISC catalog [ISC, 2016] from 2009–2016. Blue lines are the surface ruptures of the 1889 MW8.0–8.3 Chilik Earthquake [Bindi et al., 2014; Krüger et al., 2015; Abdrakhmatov et al., 2016; own mapping]. Yellow lines are the surface ruptures of the MW~8.0 1911 Chon Kemin Earthquake [Bogdanovich et al., 1914; Crosby et al., 2007; Arrowsmith et al., 2017]. The epicentre of the 1887 Verny, M7.3 earthquake is from Kondorskaya & Shebalin [1977] and fits macroseismic data from Mushketov [1890] as discussed in Tatevossian [2007]. GPS velocities relative to stable Eurasia are shown with 95% confidence ellipses [Zubovich et al., 2010]. Note the anticline in the northern outskirts of Almaty indicated by double-head arrows. Topography is from SRTM1 data.

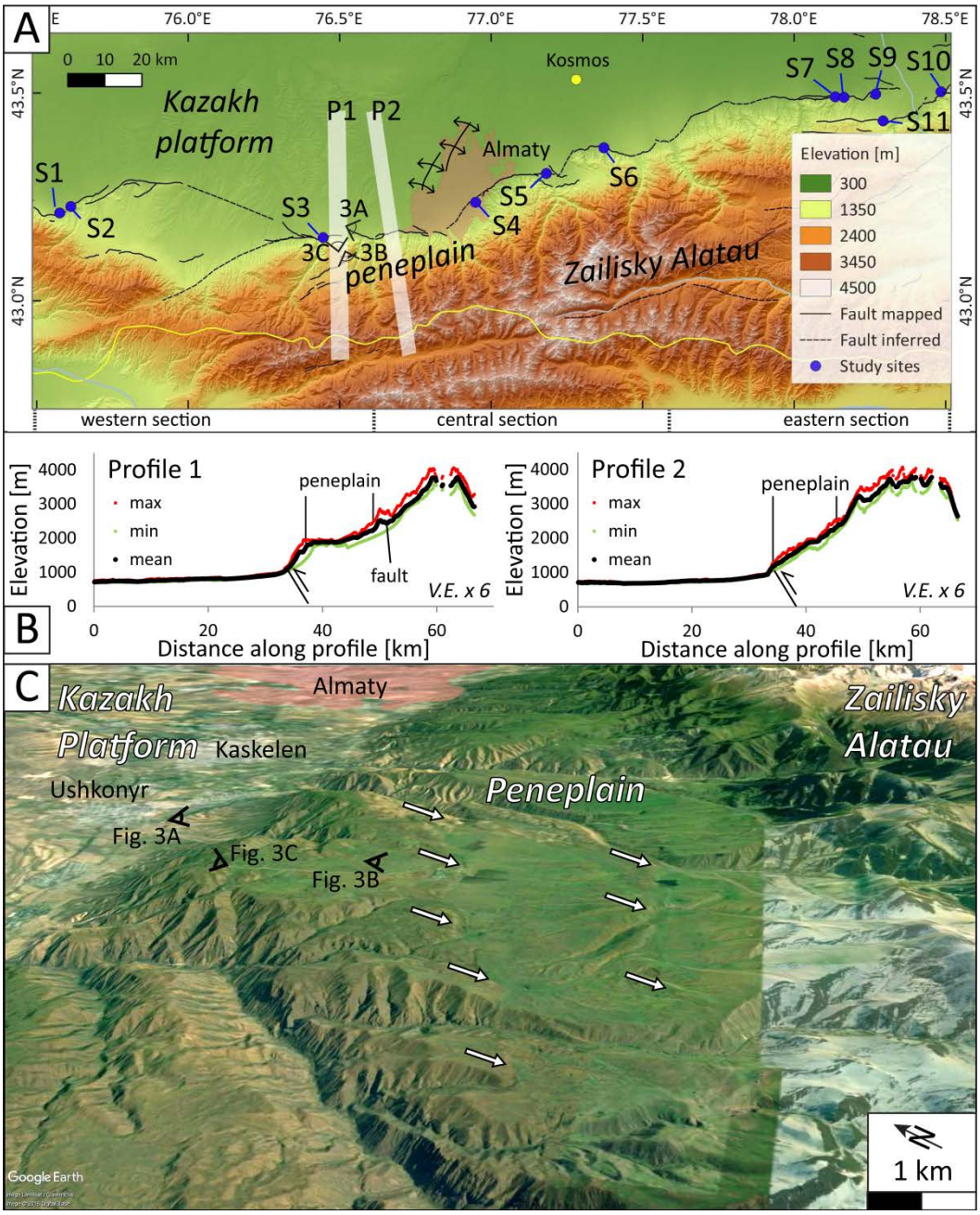

Figure 2. Morphology of our study area. (a) The ten sites S1-S11 discussed in this paper (marked with blue dots) span the entire 250 km-long Almaty rangefront. West of Almaty, anticlines strike NE (black double-headed arrows). The yellow dot marks the deformed sediments at the Kosmos site of Macklin et al. [2015]. White rectangles mark the two topographic swath profiles in b. Black symbols with capital letters mark the view direction of the photos in fig. 3. Pink shading denotes the outline extent of the urban development of Almaty. (b) Topographic swath profiles (vertically exaggerated x 6) illustrate the elevation difference between the Kazakh platform (<1,000 m) and the Zailisky Alatau (up to 4,000 m). Note the smooth peneplain surface in both profiles and the topographic high at the fault described in section 3. (c) Oblique view looking east across the Kazakh platform, the peneplain and the high Zailisky Alatau. White arrows indicate south-facing fault scarps near Ushkonyr. Imagery: GoogleEarth.

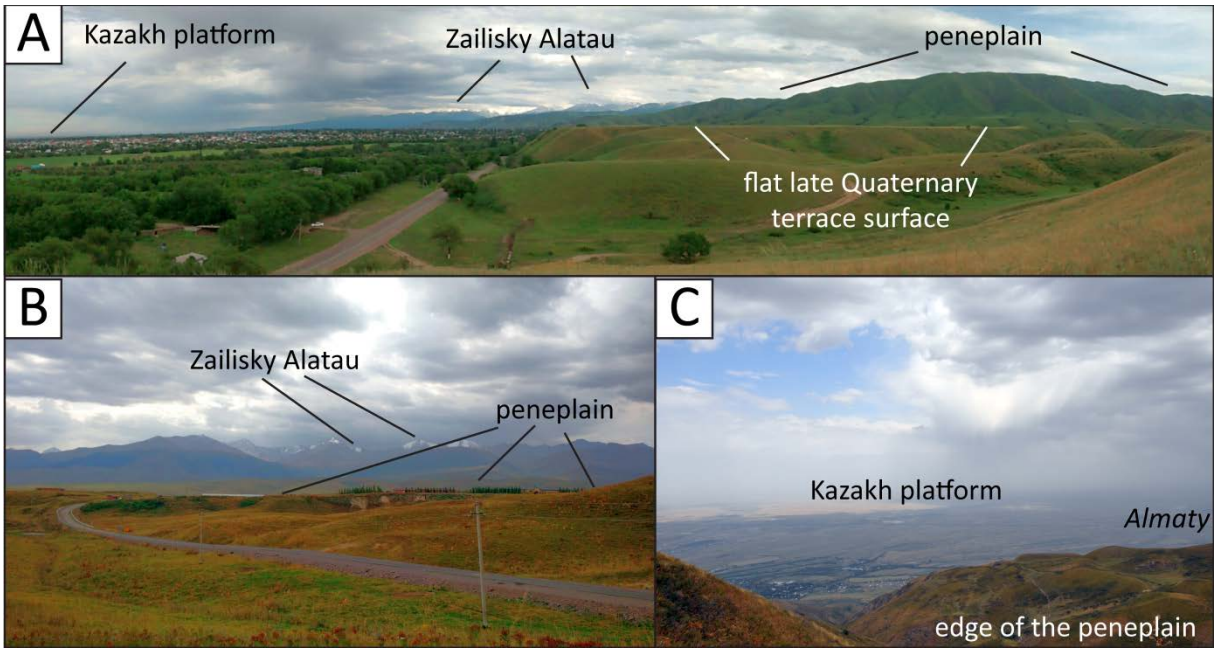

Figure 3. (a) View eastwards from the platform to the high Zailisky Alatau (N 43.170602°; E 76.531304°). Flat Quaternary terraces surfaces covered in a layer of loess are uplifted in front of the Mesozoic erosional surface. (b) View southwards from the peneplain towards the Zailisky Alatau (N 43.089242°; E 76.483833°). (c) View northwards from the peneplain towards the Kazakh platform (N 43.124964°; E 76.473749°).

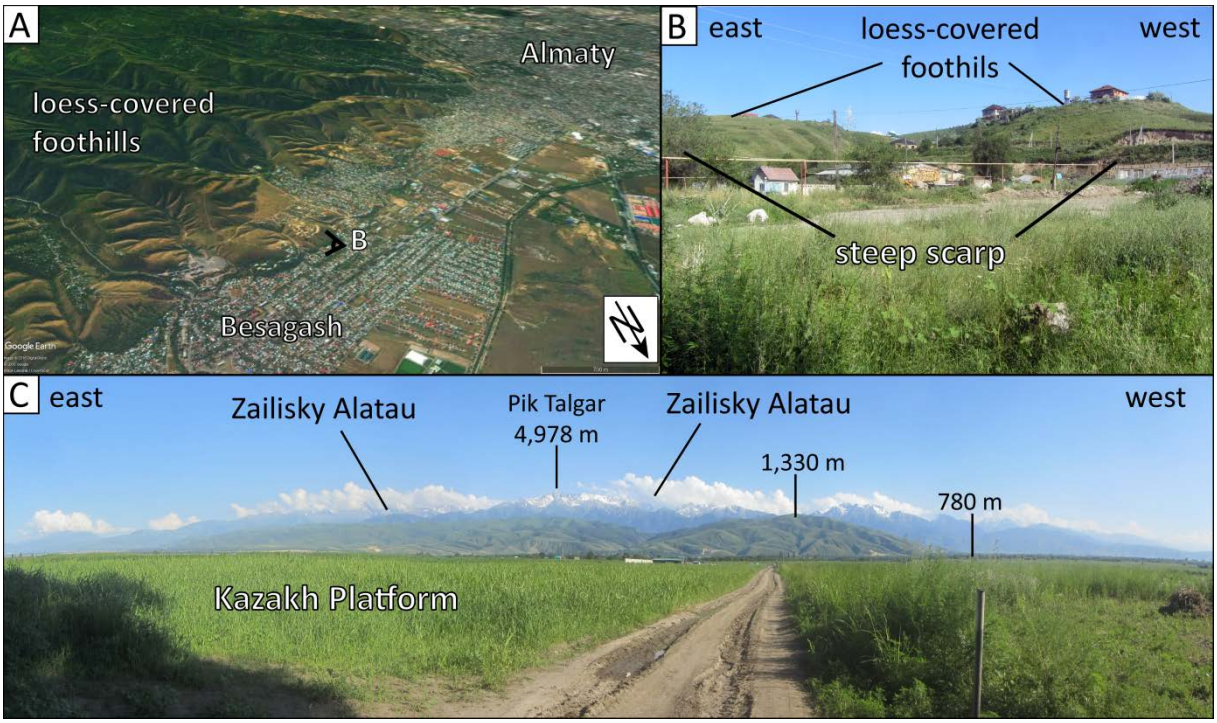

Figure 4. General geomorphic features of the Almaty rangefront. (a) The Almaty metropolitan area is growing along the rangefront, resulting in more people living directly above or close to the active faults. Urban development increasingly occupies the loess-covered foothills, for example south of Besagash. B marks the position of photo in Fig. 4b. Google Earth imagery. (b) View to the south towards the Almaty rangefront in Besagash. Note the steep scarp in front of the foothills and the new houses on top of the loess-covered hills. (c) Panorama view of the Zailisky Alatau at Talgar (77.3°E). Pik Talgar is the highest mountain in the mountain range. In front of the high Alatau loess covered hills reach up to ~1300 m. The Kazakh platform lies below 800 m.

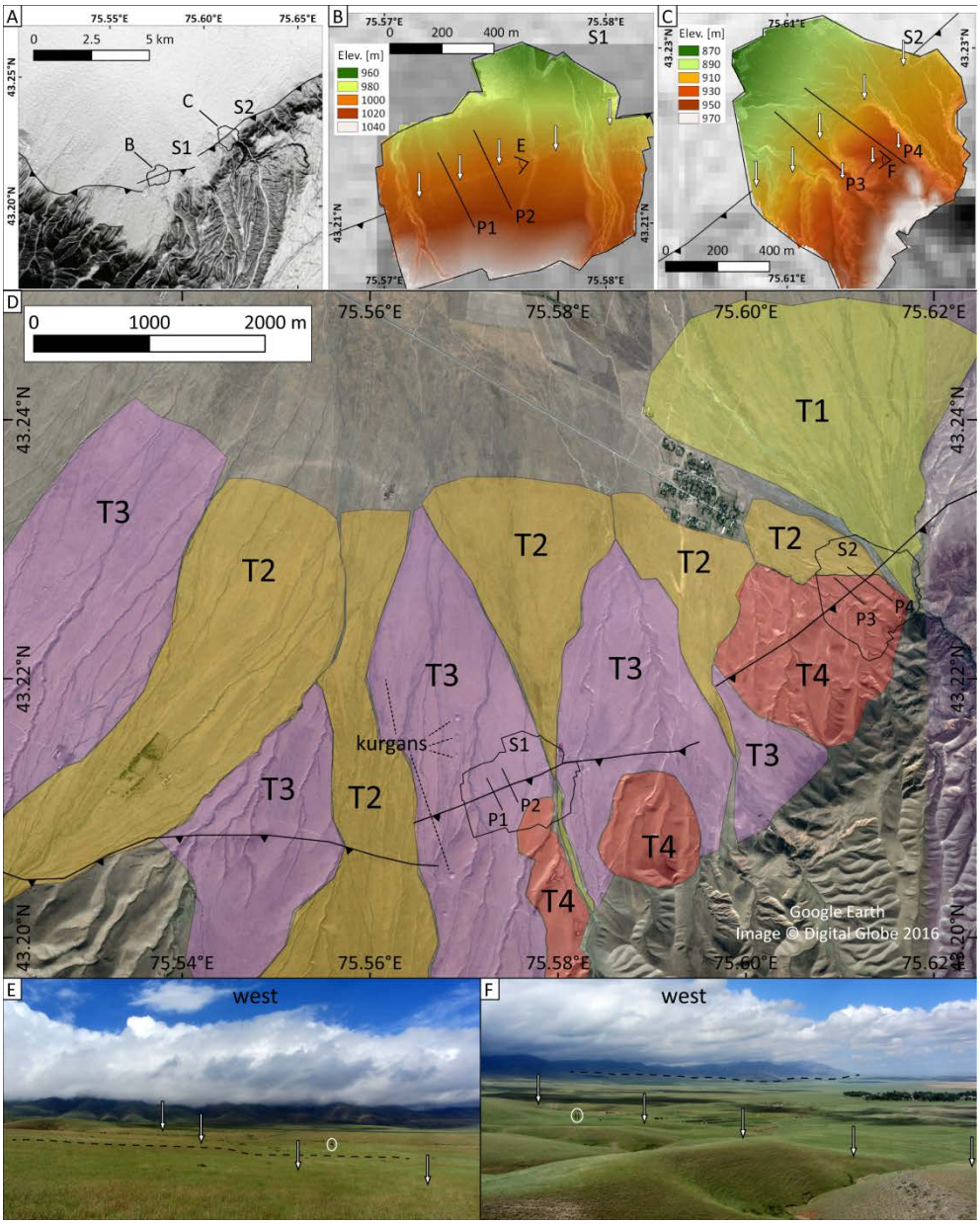

Figure 5. Akterek study sites S1 and S2. (a) Slope map based on SRTM1 data. Black lines are faults, B and C indicate the location of the two drone DEMs of S1 and S2 in Figs. 5b, 5c. (b) Drone DEM with 0.1 m resolution at S1, overlain with a semi-transparent slope map. Arrows mark the fault scarp. P1 and P2 mark the two profiles in Fig. 6a, b. E marks view direction of photo in Fig. 5e. (c) Drone DEM with 0.1 m resolution at S2, overlain with a semi-transparent slope map. Arrows mark the fault scarp. P3 and P4 mark the two profiles in Fig. 6c, d. F marks view direction of photo in Fig. 5f. The NE-SW striking linear feature visible at the NW end of P3 is a goat track. For this reason we do not label it in Fig. 6. (d) Alluvial fan surfaces T1-T4 at sites S1 and S2. T1 is the modern river bed, T4 is the oldest fan. (e) Photo of the fault scarp at S1 looking west. White arrows mark the fault trace, dashed line is profile P2, person for scale (encircled). (f) Photo of the fault scarp at S2 looking west. White arrows in the foreground mark the fault trace at the study area, dashed line traces the NW striking fault trace in the background. 5 m high poplars are encircled for scale.

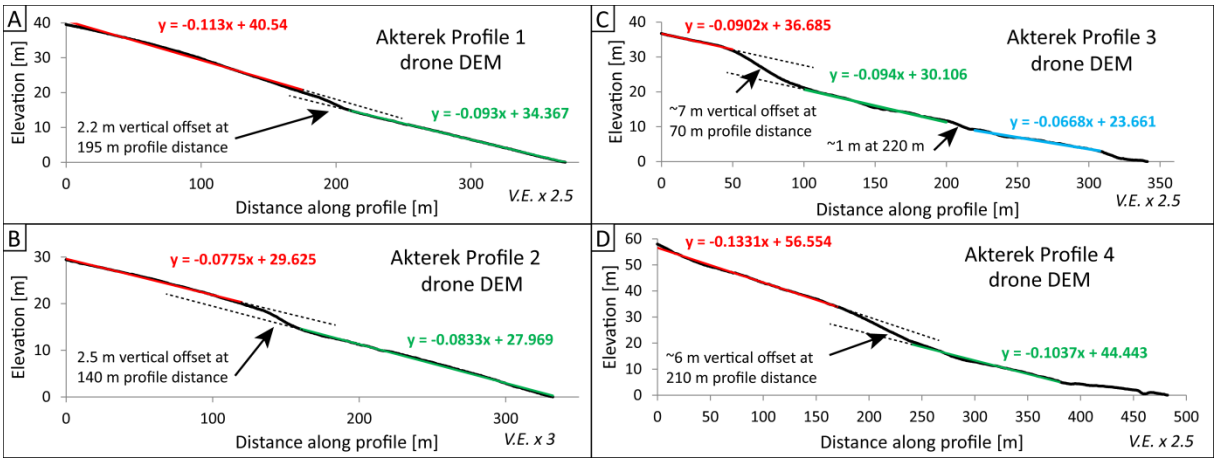

Figure 6. Topographic profiles at sites S1 and S2 near Akterek. (a) At S1 the fault scarp shows a vertical throw of 2.2 m in surface T3. (b) Fan T3 has a vertical offset of 2.5 m as observed in profile P2. (c) At S2 we observe ~7 m vertical throw at a profile distance of 70 m and another 1 m throw at 220 m profile distance in profile P3.This profile covers fan surface T4. (d) A vertical throw of ~6 m is observed in profile P4. Here the hanging wall is fan surface T4, the footwall is T3. Note that we plot elevation differences instead of absolute elevations.

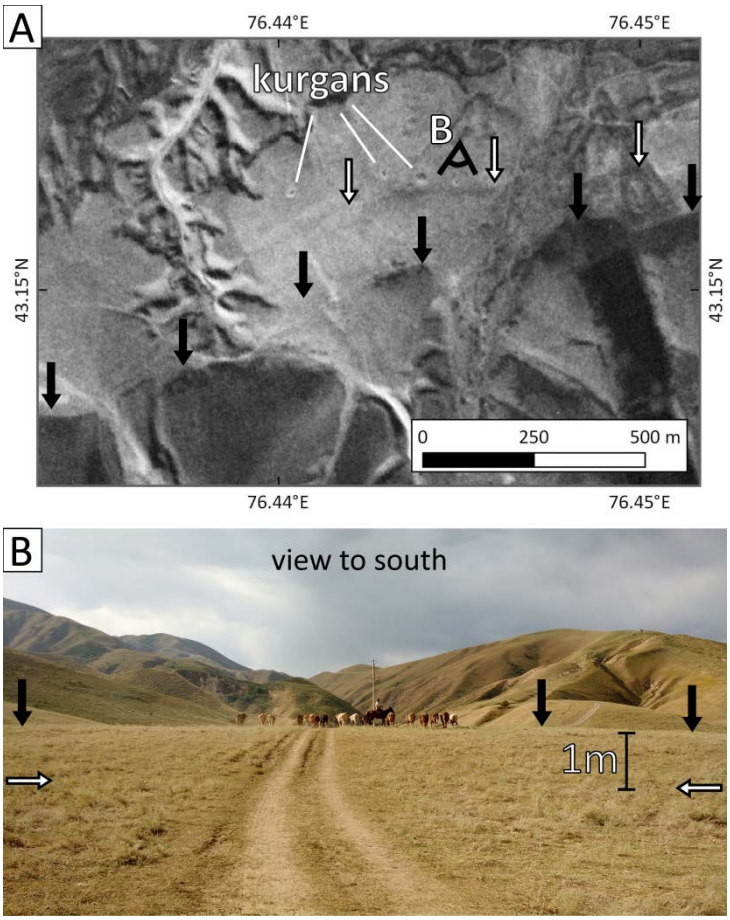

Figure 7. The Fabrichny study site (S3). (a) Declassified Corona imagery from 1969 has the advantage of pre-dating the latest phase of urban development that began in 2012/13. Black arrows indicate the ~50 m high scarp in the loess covered foothills. White arrows mark the 1 m high fault scarp. Note the kurgans N of the scarp. B marks the location of the photo shown in Fig. 7b. (b) The fault scarp (white arrows) faces to the north and is degraded.

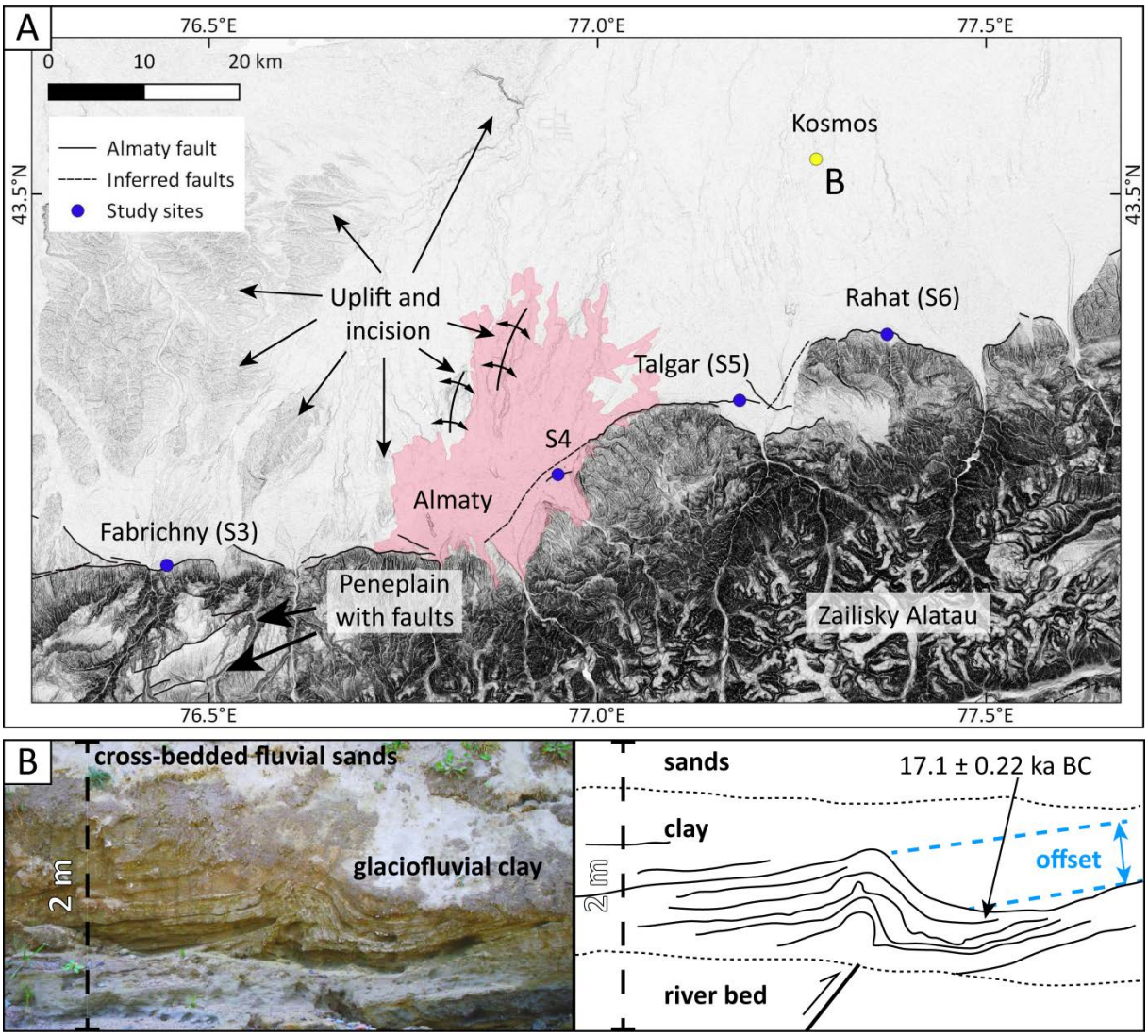

1370

1371

1372 Figure 8. (a) Slope map of Almaty from SRTM1 data. The drainage pattern to the northwest
1373 of the city indicates active uplift and consequent incision of the streams. Faulting is not
1374 confined to the rangefront, but also observed in the peneplain. Pink shading denotes the
1375 outline extent of the urban development. (b) At the Kosmos reach of river Talgar, Macklin et
1376 al. [2015] found folded and offset (blue lines) glaciofluvial deposits with an age of ~17 ka,
1377 overlain by undeformed units. Photo by Willem Toonen.

1378

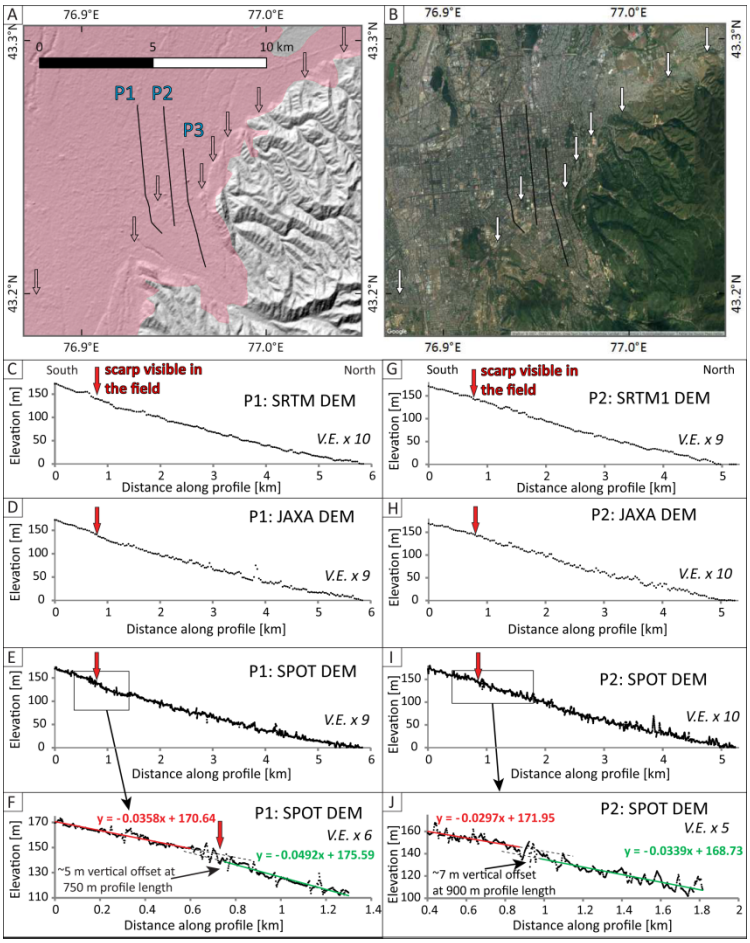

Figure 9. Fault scarps in Almaty (site S4). (a) The JAXA DEM hillshade map reveals a linear break in slope across the alluvial fan (arrows). P1-3 mark the location of the topographic profiles along main roads. Pink shading denotes the outline extent of the urban development. (b) Same map as in Fig. 9a but with Google Earth satellite imagery. (c) Topographic profile P1 from SRTM1 data. (d) Topographic profile P1 from JAXA data. (e) Topographic profile P1 from the SPOT DEM. (f) Zoom into the SPOT DEM along P1. (g) Topographic profile P2 from SRTM1 data. (h) Topographic profile P2 from JAXA data. (i) Topographic profile P2 from the SPOT DEM. (j) Zoom into the SPOT DEM along P2. In all profiles the red arrow marks the location of the scarp as seen in the field.

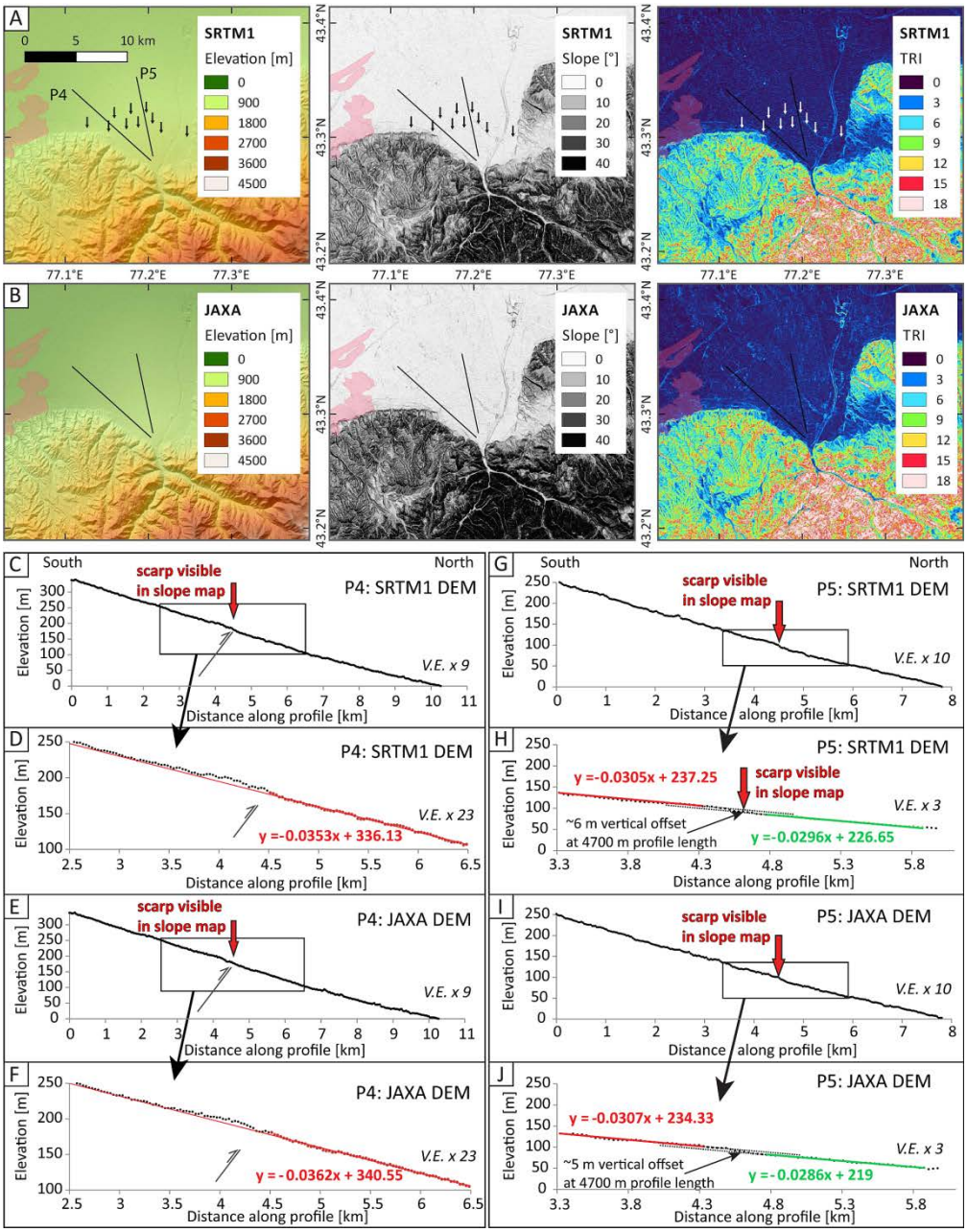

Figure 10. Active faulting at Talgar (site S5) scarps in Almaty. (a) Elevation, slope, and TRI map of Talgar based on SRTM1 data. Arrows indicate breaks in slope that we interpret as fault scarps. P4 and P5 are the profiles shown in Fig. 10c-j. Pink shading denotes the outline extent of the urban development. (b) Same map as in Fig. 10a but using the JAXA DEM. (c) Topographic profile P4 from SRTM1 data. (d) Zoom into the section in which we see the scarp in the DEM. Note the ~1 km wavelength folding at this site. Only the red data points were used to calculate the linear fit. (e) Topographic profile P4 from the JAXA DEM. (f) Zoom into the section in which we see the scarp in the DEM. Note the ~1 km wavelength folding at this site. Only the red data points were used to calculate the linear fit. (g) Topographic profile P5 from SRTM1 data. (h) Zoom into the section in which we see the scarp in the DEM. Note the ~6 m vertical offset. (i) Topographic profile P5 from the JAXA DEM. (j) Zoom into the section in which we see the scarp in the DEM. Note the ~5 m vertical offset. In all profiles the red arrow marks the location of the scarp as seen in the slope map.

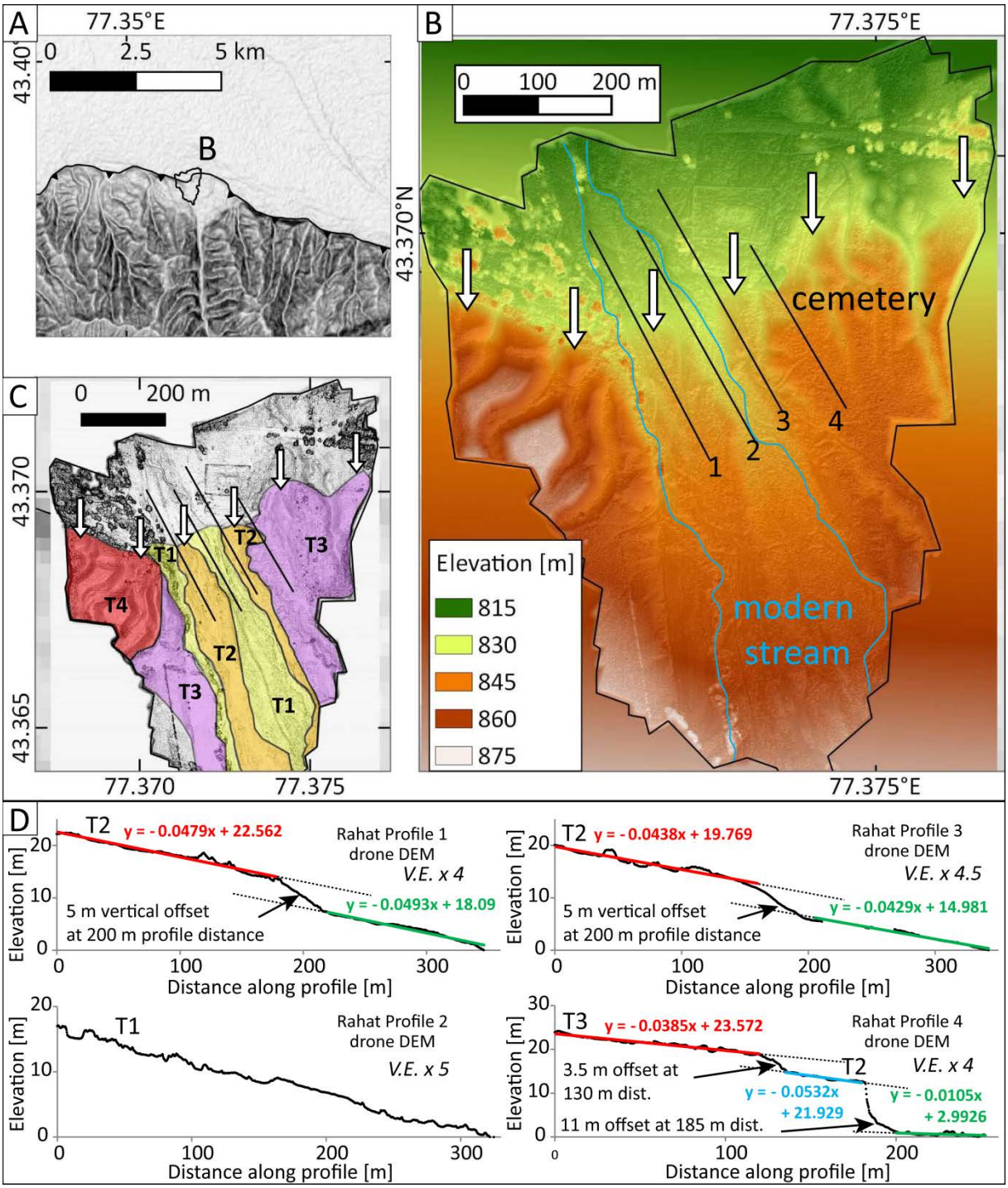

Figure 11. Study site S6 near Rahat. (a) Location of the study site (black outline) on a SRTM1 slope map. (b) Drone DEM of the study site overlain with a semi-transparent slope map with the four profiles shown in Fig. 11d. White arrows mark the fault scarp. (c) Slope map from the drone DEM with the three river terraces T1-T4 (youngest-oldest). (d) Topographic profiles 1-4 extracted from the drone DEM.

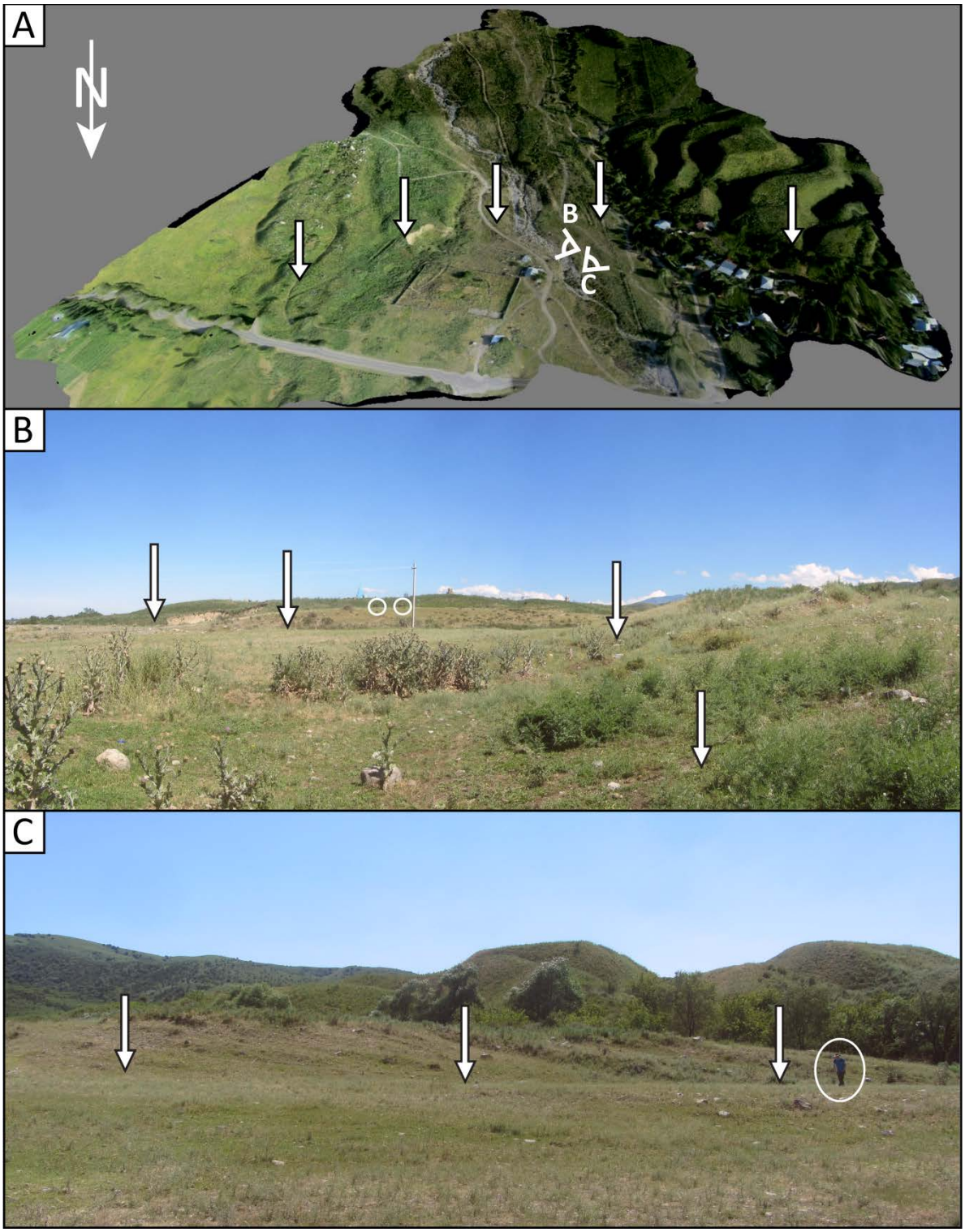

Figure 12. Field photos of the scarp (white arrows) in Rahat. (a) Aerial imagery draped over the drone DEM. Capital letters indicate location and direction of photos in Fig. 11b, c. (b) View east towards the cemetery. Horses encircled for scale. (c) View to the southwest towards profile 1 in Fig. 11. Person encircled for scale.

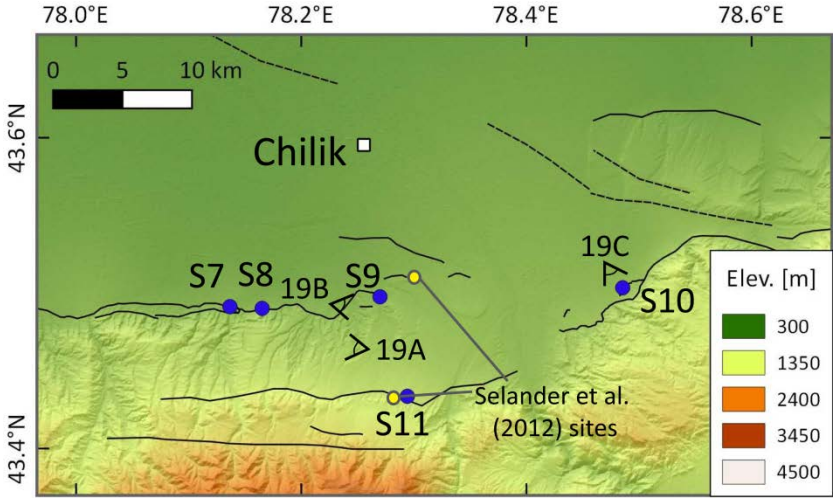

Figure 13. Investigation sites at the eastern end of the Zailisky-Alatau rangefront near Chilik. Overview map showing the study sites S7-S11 (blue dots). Yellow dots indicate the slip rate site of Selander et al. [2012]. Black lines are active reverse faults mapped remotely or in the field. Dashed lines are active faults inferred from gaps in between the mapped fault traces. Capital letters and symbols mark the location of photos in Fig. 19.

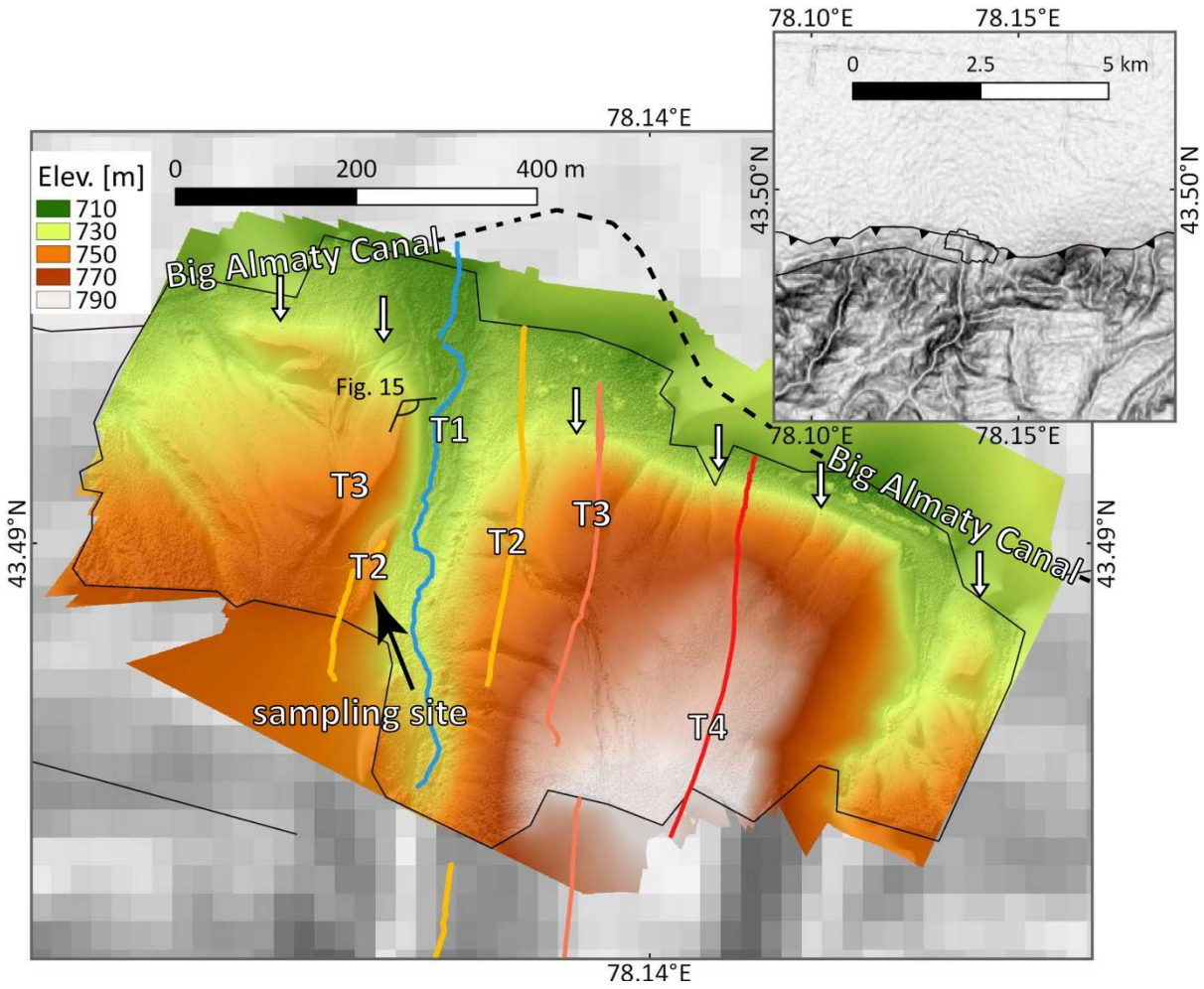

1426

1427

1428 Figure 14. Study site S7. Inset shows the location of the site at the rangefront. The large map
1429 shows the drone DEM overlain with a semi-transparent hillshade. Coloured lines are the
1430 DGPS profiles on three different terrace levels, see Fig. 16 for results. The blue line is the
1431 modern stream incising into T1. The Big Almaty Canal is indicated by the dashed black line.
1432 White arrows mark the fault trace. See Fig. 17 for a detailed view of the sampling site.

1433

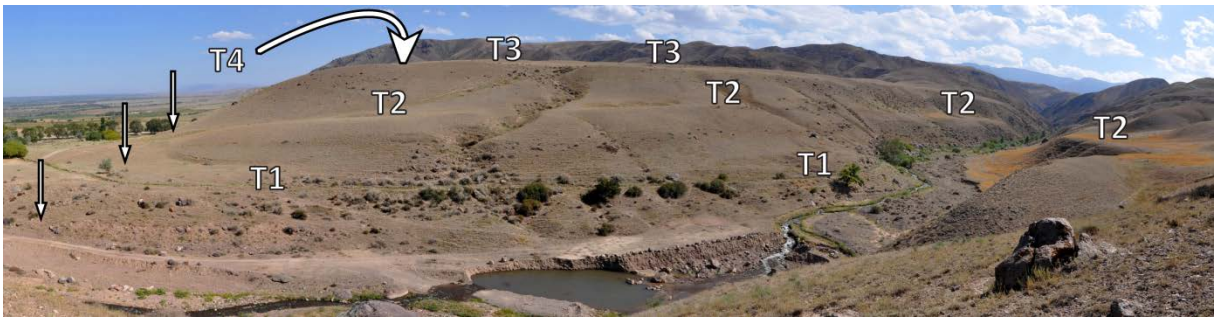

Figure 15. Panorama photo of the terrace levels at site S7 looking east. T4 is hidden behind T3 and not visible in this picture. The sampling site is not visible here as it is located below T3 in the foreground on the west bank of the stream. White arrows denote fault trace.

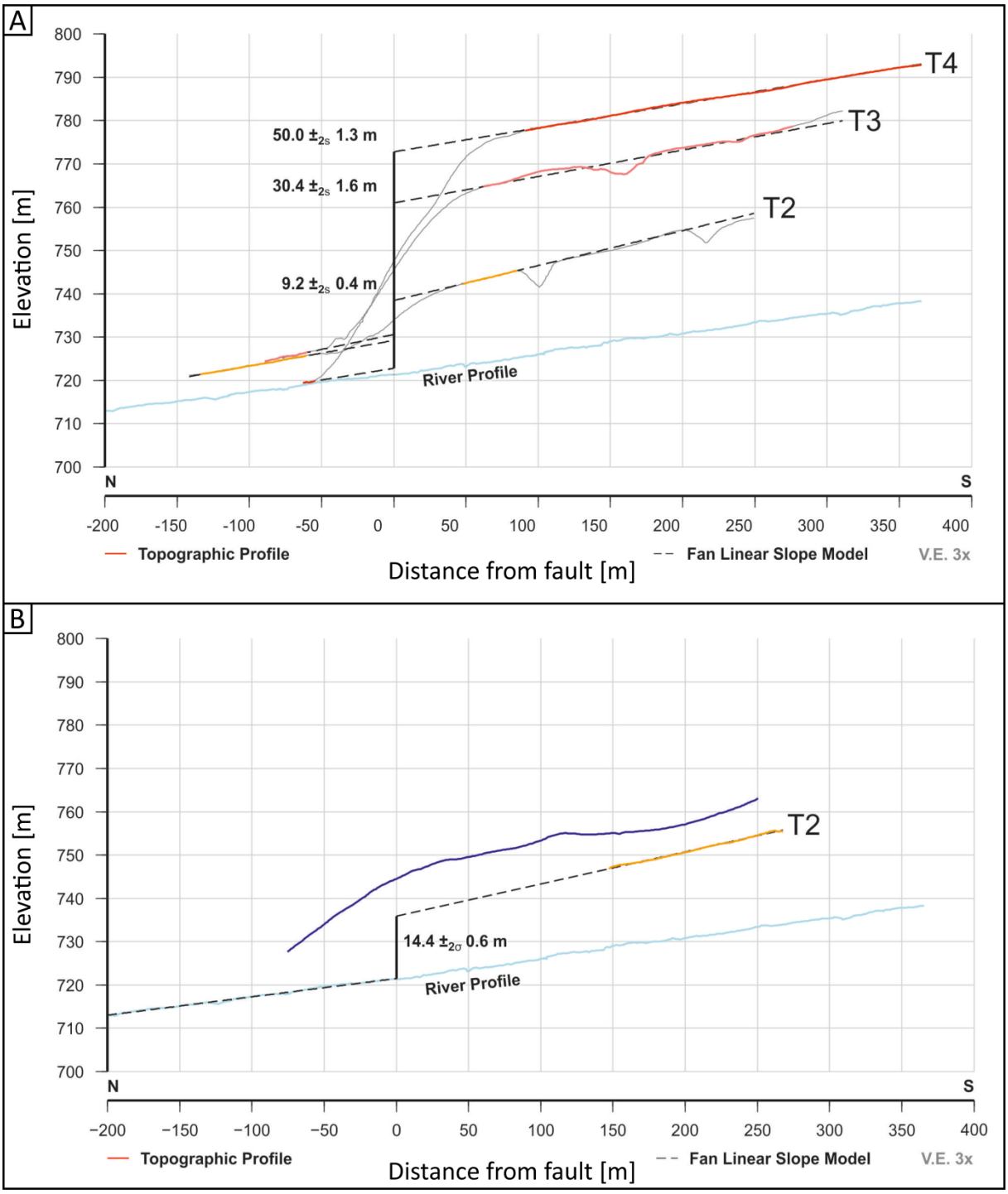

Figure 16. DGPS profiles across the different terraces with 3 x vertical exaggeration; see Fig. 14 for location. (a) Terraces on the eastern bank of the stream colour coded as in Fig. 14. We assumed a linear slope that we projected to the fault and then measured the vertical offset with respect to the footwall terrace or modern stream level. Fault location was set to the steepest section of the scarp. (b). Terrace profile T2 at the study site on the west bank of the stream. The purple line marks a remnant of a surface west of terrace T2.

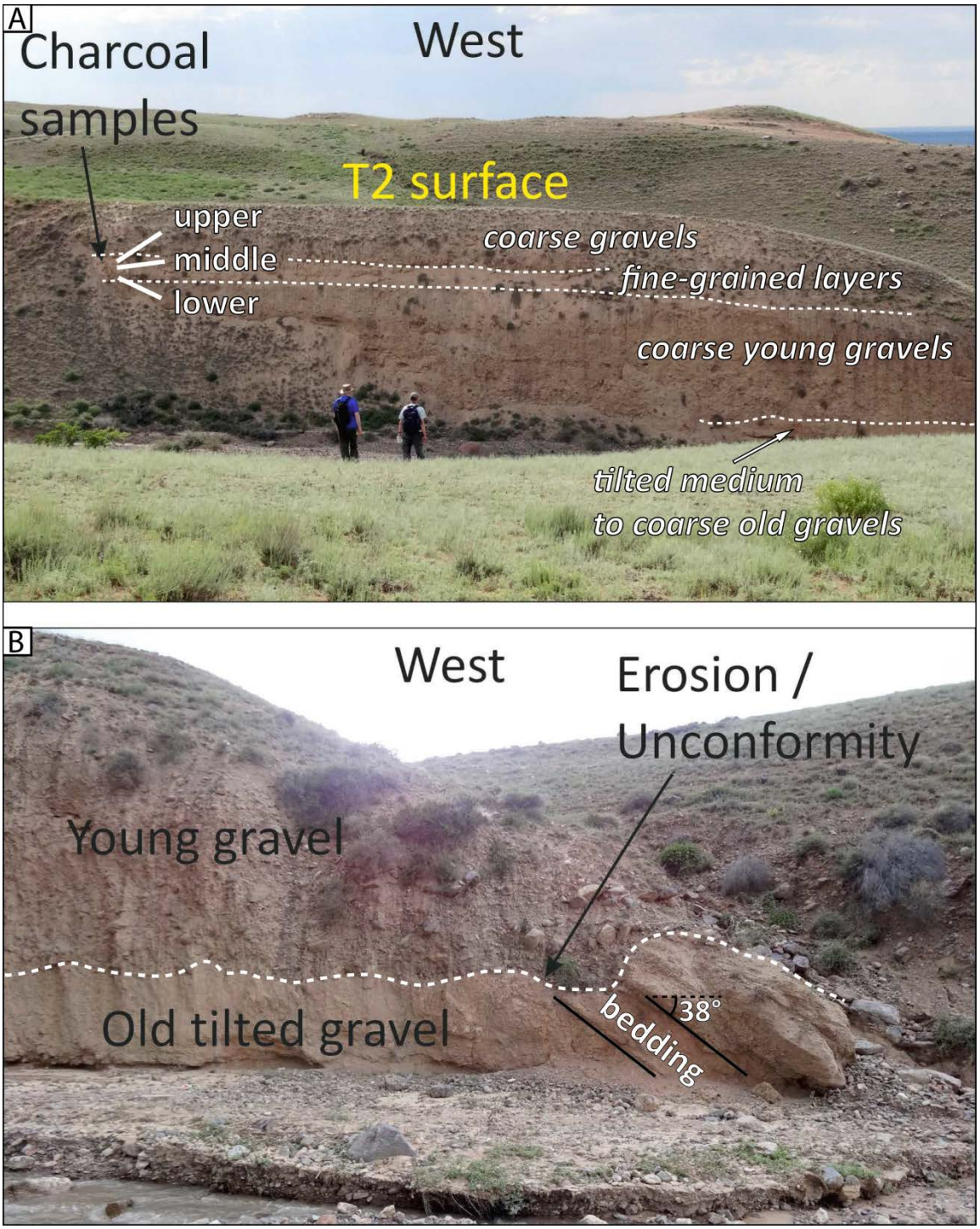

Figure 17. Sample location for the slip rate measurements. (a) Terrace T2 is covered by a 1 m thick gravel layer that overlies a fine-grained sequence. Three charcoal samples were taken from various depths below this gravel layer: chilik-2016-upper (0.8 m below); chilik-2016-middle (0.95 m below), and chilik-2016-lower (1.7 m below). See Table 2 for results. View is to the west. (b) The northern tip of T2 exhibits an erosional unconformity, separating Holocene gravels on top from N-tilted finer gravels of unknown age.

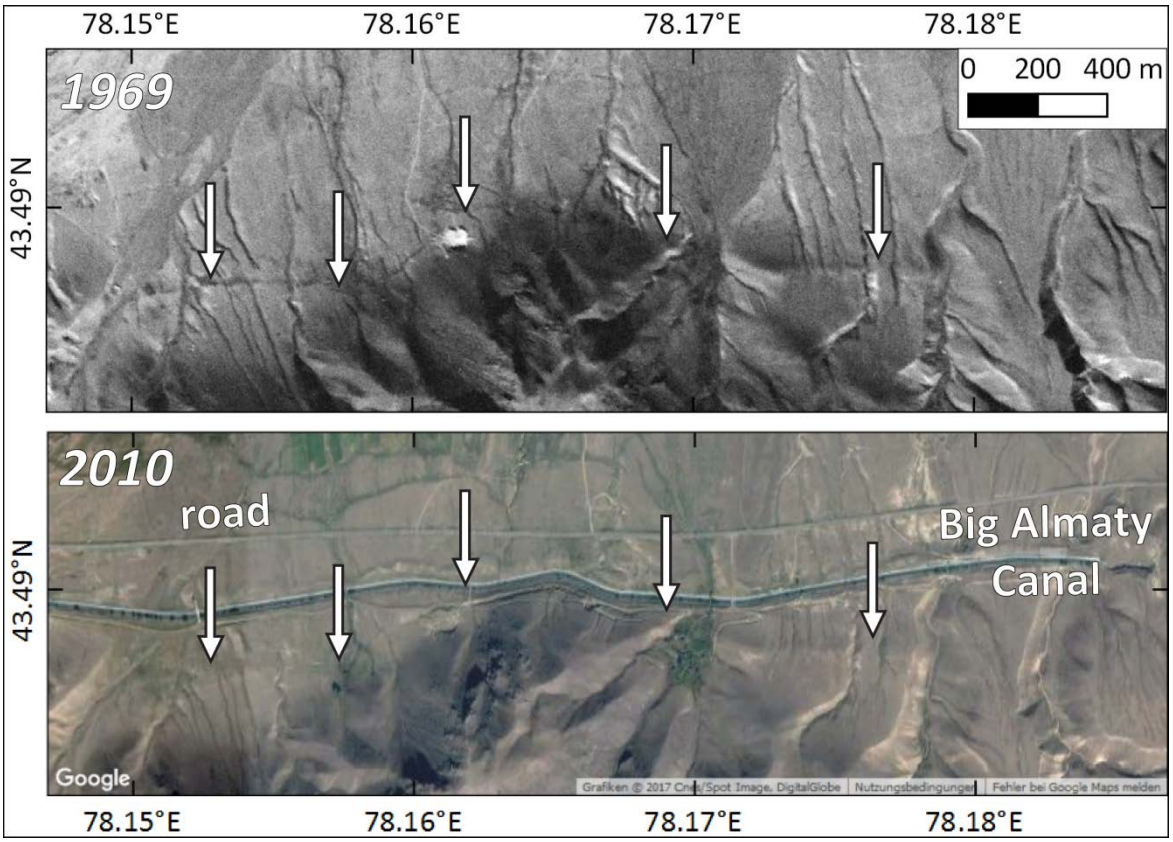

Figure 18. Site S8 at the Big Almaty Canal. A fault scarp is visible in declassified Corona satellite imagery from 1969. GoogleEarth imagery from 2010 shows that the canal was built along, and in parts on, the fault scarp.

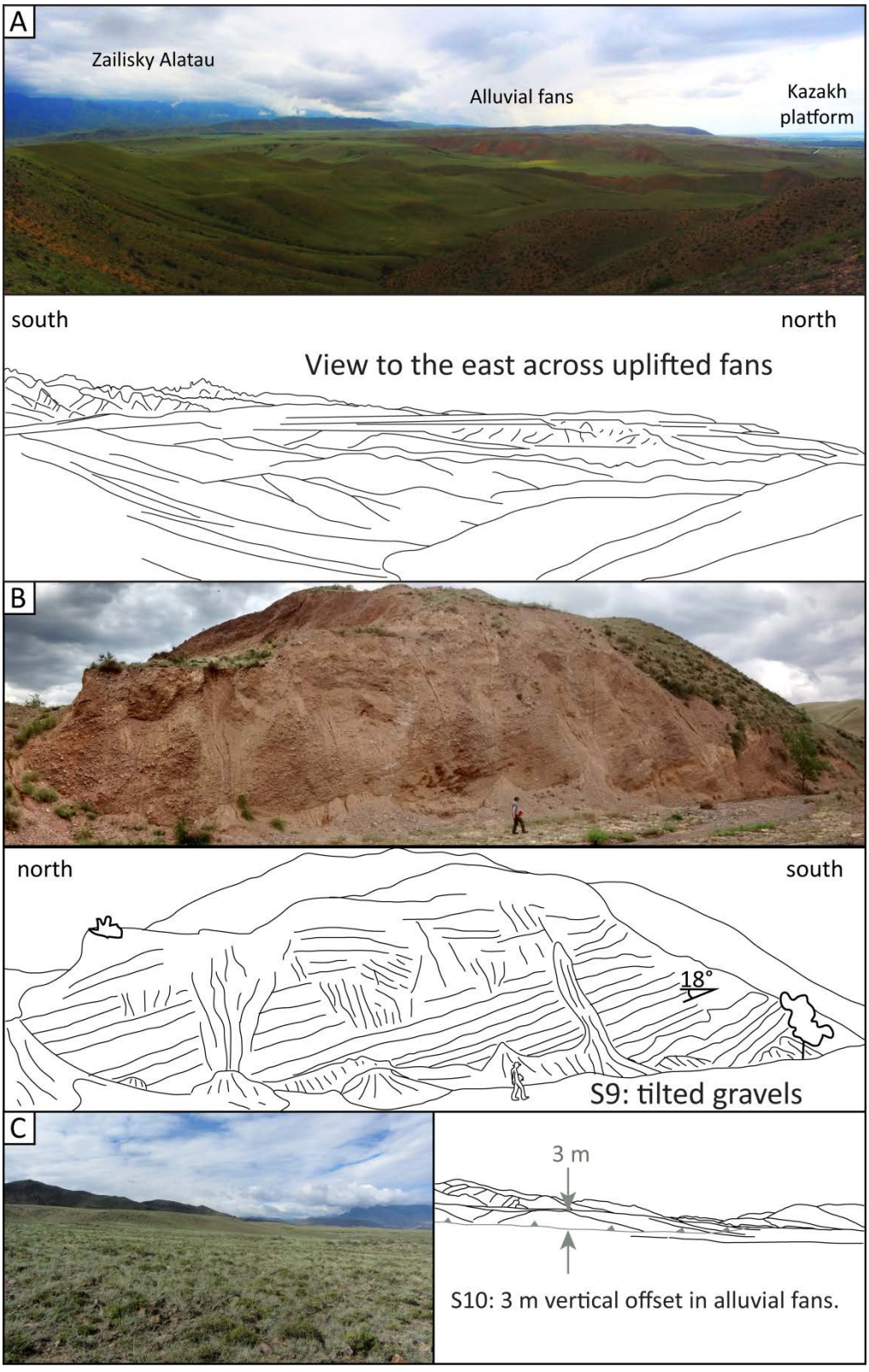

Figure 19. (a) Stitched field photo and sketch drawing of uplifted terraces in between the Zailisky Alatau rangefront and the Kazakh platform. (b) Field photo and sketch drawing of tilted gravel layers that crop out in a river bank at site S9. The gravels dip 18° to the north and are bound to the north by a reverse fault. (c) Field photo and sketch drawing of the fault scarp at site S10 where we found alluvial fans with 3 m vertical offset. See Fig. 13 for location.

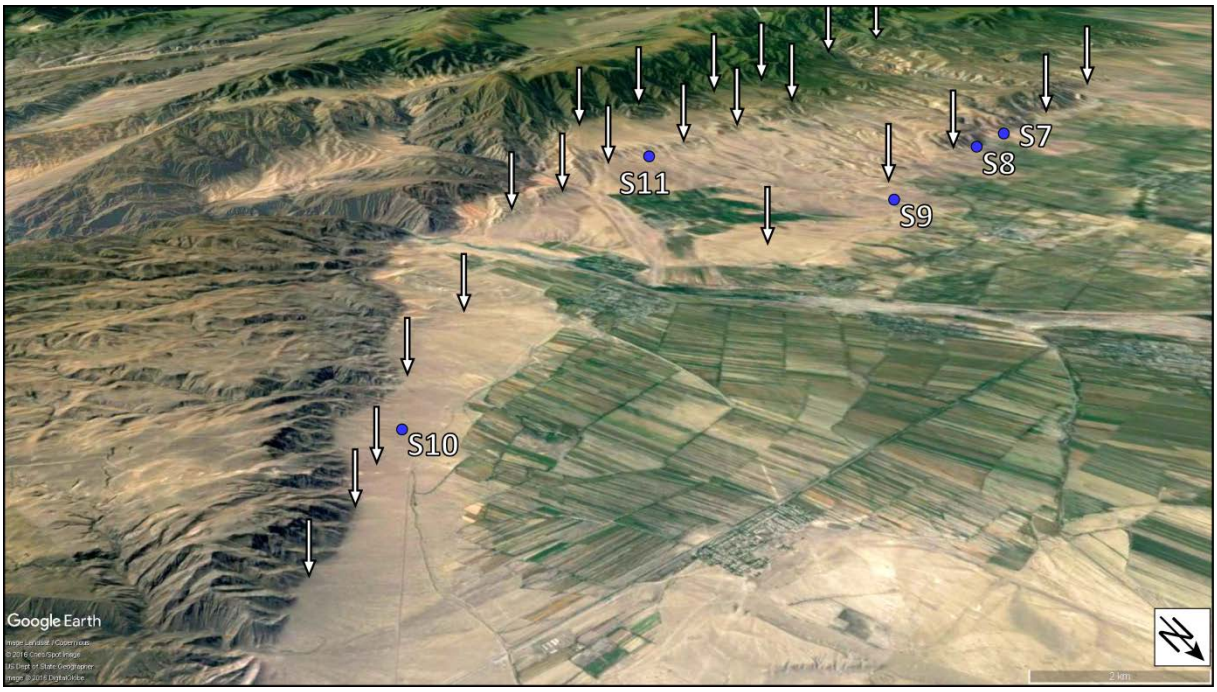

Figure 20. Oblique view to the southwest. Three distinct fault traces (white arrows) are visible in between the Kazakh platform and the Zailisky Alatau. The folded terraces in the centre of the plateau near S11 and the fault in the north were investigated by Selander et al. [2012]. Blue dots indicate the study sites S7-S11 in the eastern part of the Almaty rangefront fault. Imagery: GoogleEarth.

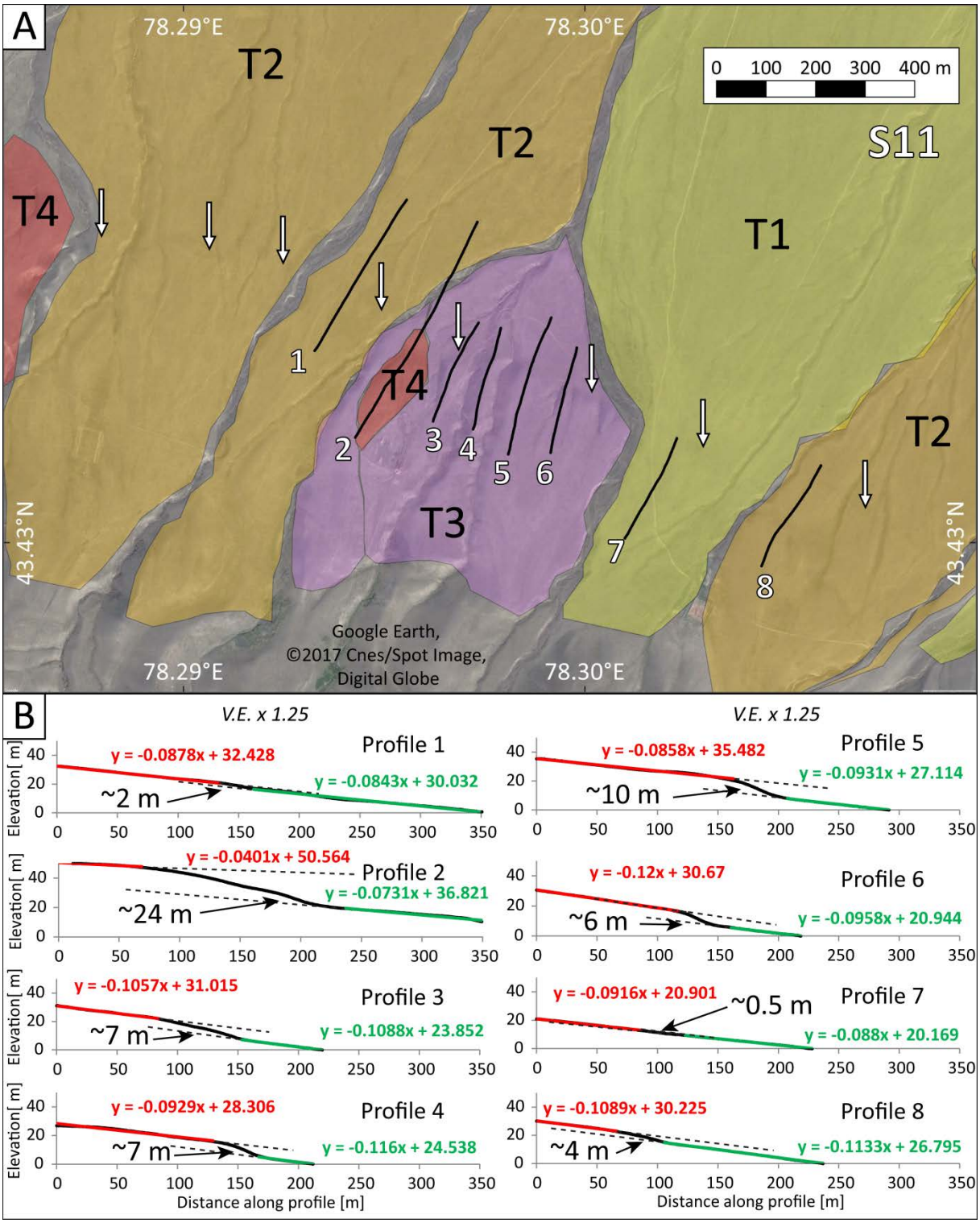

Figure 21. Study site S11. (a) Map showing the fault scarp (white arrows) and the four different fan levels T1-T4 (youngest – oldest) in Google Earth. Black lines are the eight DGPS profiles presented in Fig. 21b. (b) Topographic profiles 1-8 (vertically exaggerated). Note that the elevation differences along profile rather than absolute elevations are plotted for comparability. Black number indicates vertical throw measured at the position marked by the black arrow in each profile. Profile 7 is located on T1, profiles 1 and 8 measure the offset of fan T2. Alluvial fan T3 is probed by profiles 3-6, and profile 2 crosses the oldest fan T4.

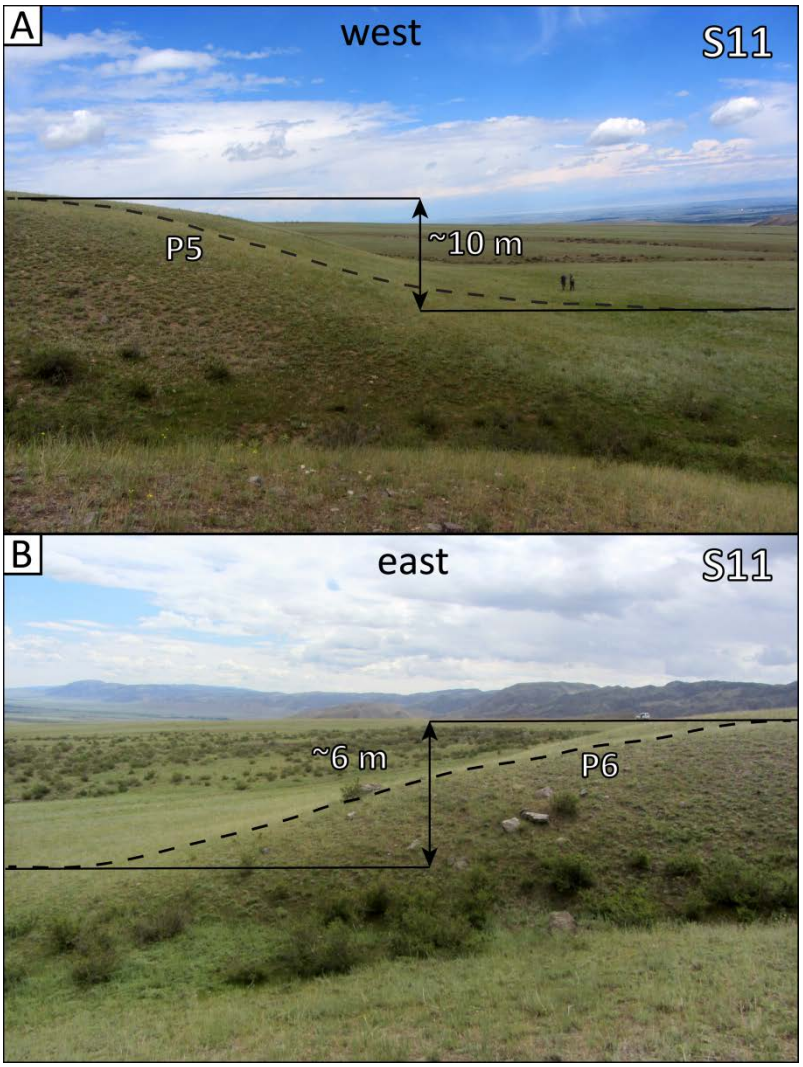

Figure 22. Fault scarps in fan T3 at site S11. (a) Photo looking west to profile P5. Here we measured ~10 m vertical offset with DGPS. Note the two geologists for scale. (b) Photo looking east to P6 with ~6 m of vertical offset. Both scarps probably record multiple earthquake events.

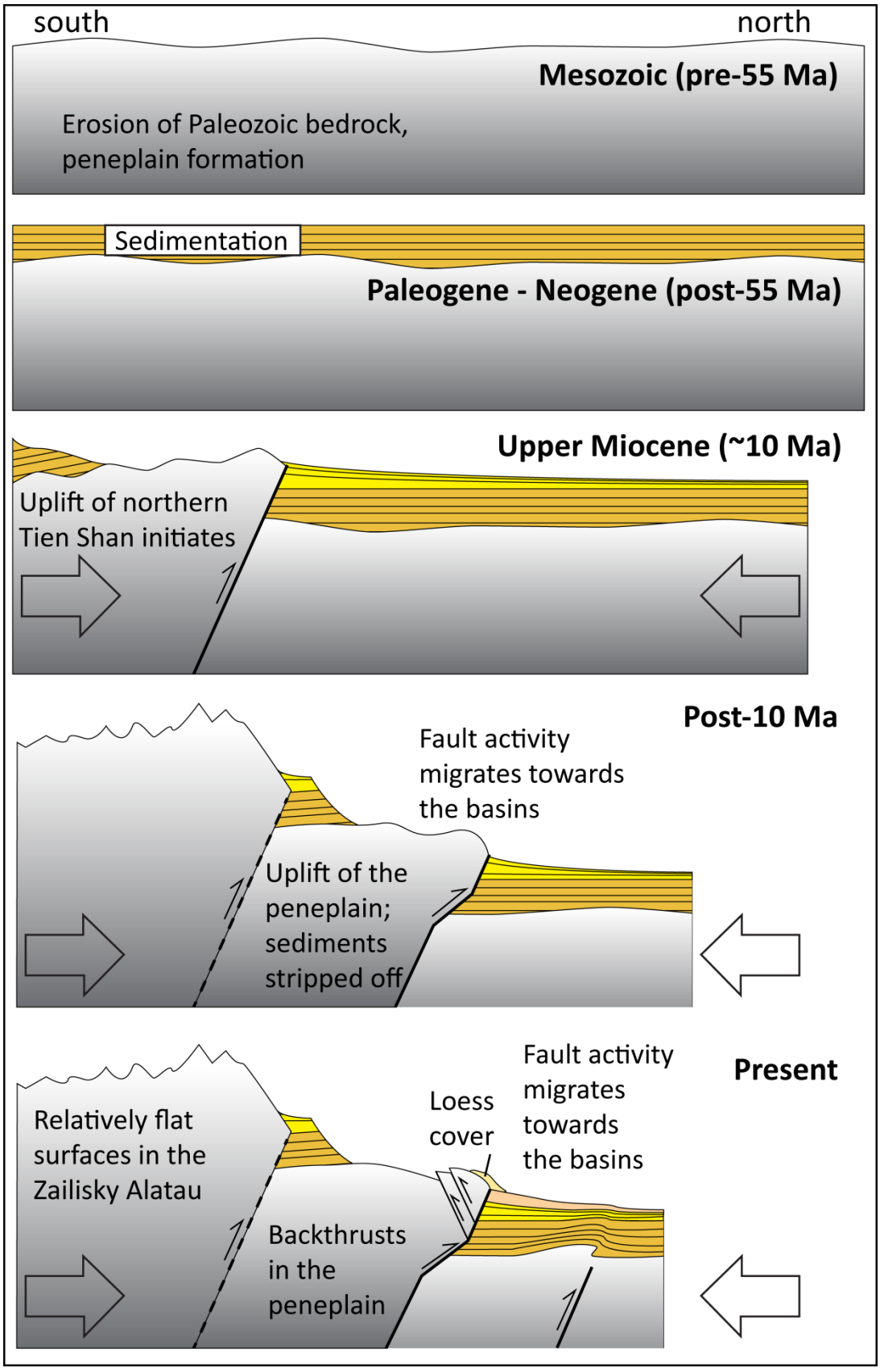

Figure 23. Generalized evolution of the Zailisky Alatau since the Mesozoic, not to scale. Solid lines mark active faults, dashed lines mark faults that are at less active.

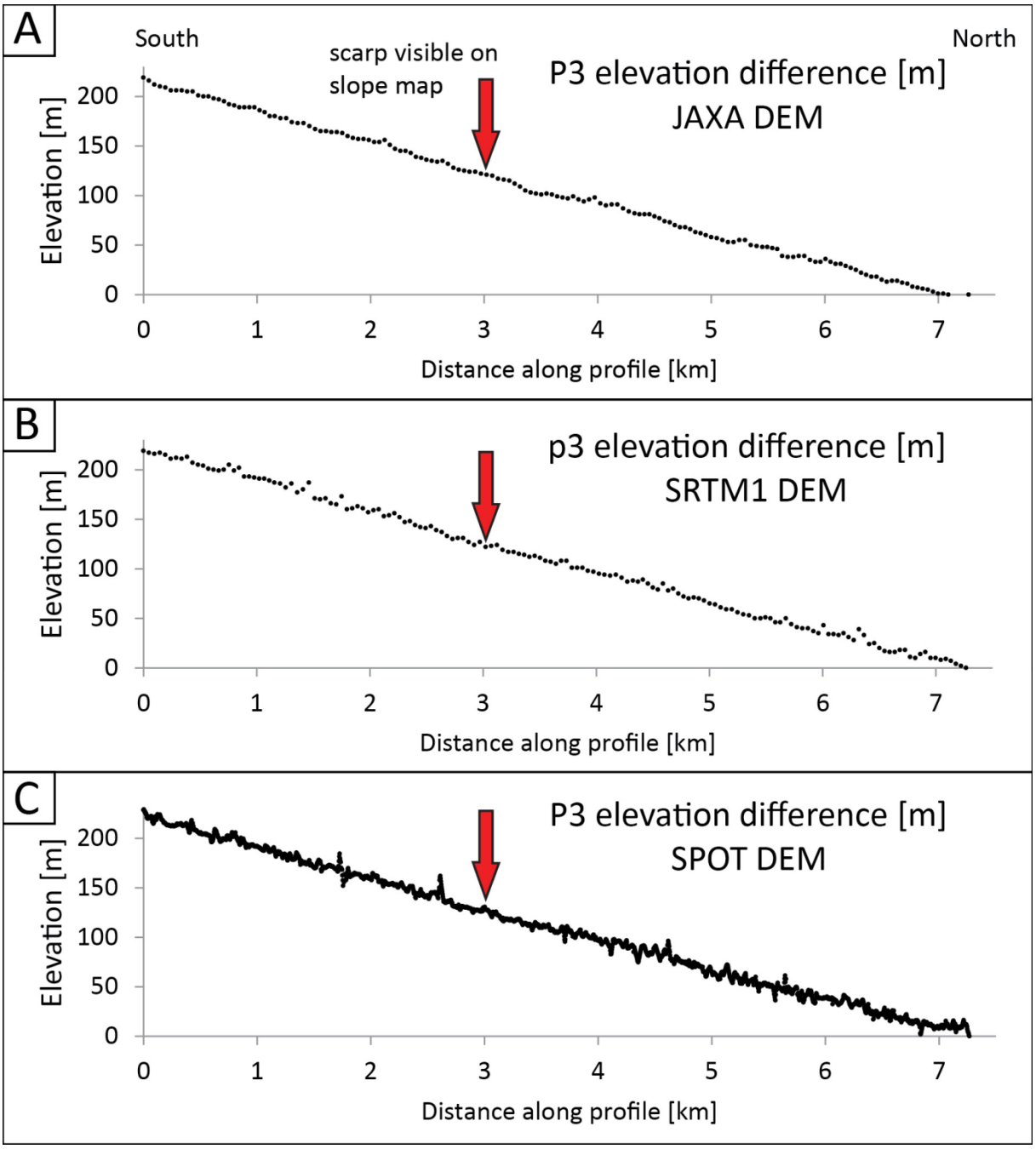

Appendix 1: JAXA, STRTM, and SPOT DEMs from profile P3 in Almaty (site S4). No vertical offset was recorded in these profiles. See figure 9 for location.